

# Taming SAM3 in the Wild: A Concept Bank for Open-Vocabulary Segmentation

Gensheng Pei<sup>1</sup> Xiruo Jiang<sup>2</sup> Yazhou Yao<sup>3</sup> Xiangbo Shu<sup>3</sup> Fumin Shen<sup>4</sup> Byeungwoo Jeon<sup>1</sup>

## Abstract

The recent introduction of SAM3 has revolutionized Open-Vocabulary Segmentation (OVS) through *promptable concept segmentation*, which grounds pixel predictions in flexible concept prompts. However, this reliance on pre-defined concepts makes the model vulnerable: when visual distributions shift (*data drift*) or conditional label distributions evolve (*concept drift*) in the target domain, the alignment between visual evidence and prompts breaks down. In this work, we present CONCEPTBANK, a parameter-free calibration framework to restore this alignment on the fly. Instead of adhering to static prompts, we construct a dataset-specific concept bank from the target statistics. Our approach (i) anchors target-domain evidence via class-wise visual prototypes, (ii) mines representative supports to suppress outliers under data drift, and (iii) fuses candidate concepts to rectify concept drift. We demonstrate that CONCEPTBANK effectively adapts SAM3 to distribution drifts, including challenging natural-scene and remote-sensing scenarios, establishing a new baseline for robustness and efficiency in OVS. Code and model are available at <https://github.com/pgsmall/ConceptBank>.

## 1. Introduction

Open-vocabulary segmentation (OVS) (Zhao et al., 2017; Zhou et al., 2022a; Xu et al., 2022b; Mukhoti et al., 2023) has fundamentally shifted visual recognition from closed-set taxonomies to language-driven generalization. By leveraging the semantic richness of contrastive vision-language models (VLMs) (Radford et al., 2021; Jia et al., 2021), modern OVS approaches allow users to segment arbitrary categories using free-form text. Among these, SAM3 (Carion

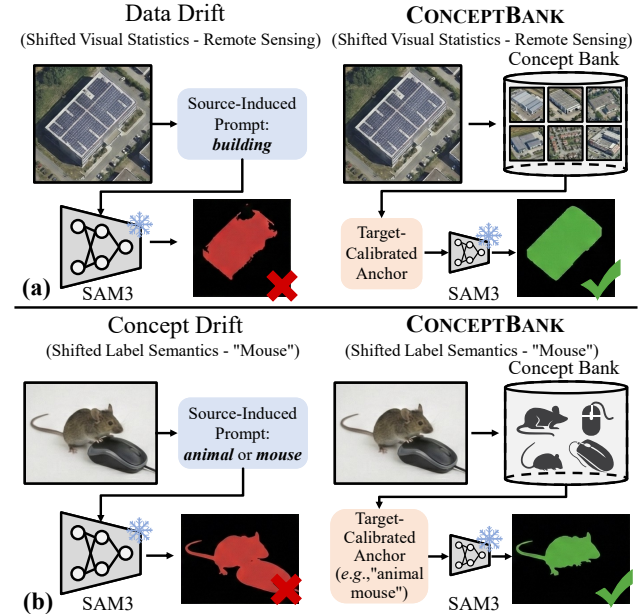


**Figure 1. Data drift and concept drift in SAM3.** We contrast the segmentation outputs of vanilla SAM3 and our CONCEPTBANK under two failure patterns: (a) *data drift* (shifted visual statistics) and (b) *concept drift* (shifted label semantics). CONCEPTBANK restores prompt-mask alignment by replacing static source-induced prompts with target-calibrated anchors from a Concept Bank.

et al., 2026) stands as a pivotal representative. Through its *promptable concept segmentation* mechanism, SAM3 does not merely classify regions; it steers the mask generation process directly via flexible concept prompts, offering a compelling vision of a reusable, *segment-anything* foundation model in the open-vocabulary segmentation regime.

However, the promise of a universal, drop-in segmenter encounters a harsh reality when deployed in the wild: the assumption that a static text embedding (the prompt) remains a valid anchor for visual concepts across diverging domains is often flawed. While SAM3 possesses powerful generalization capabilities, its reliance on pre-defined concepts renders it vulnerable to distribution drifts. As illustrated in Fig. 1, this fragility manifests as two distinct yet interconnected failure patterns, as follows:

- *Data Drift* ( $P_{\mathcal{S}}(X) \neq P_{\mathcal{D}}(X)$ ): The visual statistics of the target domain  $\mathcal{D}$  often diverge significantly from the source pre-training distribution  $\mathcal{S}$ . For instance, in remote sensing or medical imaging, spectral characteristics,

bird’s-eye viewpoints, and complex background textures perturb the geometry of the dense visual features (Kore et al., 2024). Since SAM3 relies on similarity-based matching, geometric distortions cause valid visual evidence to drift away from their corresponding text anchors, leading to segmentation collapse or hallucination.

- *Concept Drift* ( $P_S(Y|X) \neq P_D(Y|X)$ ): The conditional semantics of a label are not immutable; they evolve with context (Lu et al., 2018). A class name such as “*mouse*” can denote a computer peripheral in one dataset but refer to a mammal in another domain, leading to incompatible label semantics despite sharing the same name. When a static prompt embedding carries a pre-training-dominant interpretation into a target domain governed by a different labeling rule, the model suffers from semantic misalignment, even if the visual features are robust.

Current approaches to mitigate these shifts typically fall into two directions. On one hand, *model fine-tuning* or adapter learning can realign the visual backbone, but this sacrifices the training-free efficiency of foundation models, introduces bias toward the adapted domains, and requires additional optimization and compute (Xu et al., 2022b; Li et al., 2022a; Ghiasi et al., 2022; Xie et al., 2024; Cho et al., 2024; Luo et al., 2023; Wu et al., 2024; Barsellotti et al., 2025). On the other hand, *prompt engineering* attempts to tweak the text side manually, but this is a blind process. It ignores the actual statistical distribution of the target data and often devolves into trial-and-error heuristics. Prompt learning methods improve conditioning when training is allowed (Zhou et al., 2022b; Khattak et al., 2023; Pratt et al., 2023), yet they still rely on an explicit optimization stage that is misaligned with the plug-and-play deployment goal. To bridge this gap, we argue for a *data-centric calibration* perspective. Rather than modifying the heavy visual backbone or guessing the optimal text template, we propose to *tame* the model (*i.e.*, SAM3) by recalibrating its concept representations using the target data itself. If the visual evidence shifts, the linguistic anchors must shift to meet it.

In this work, we present **CONCEPTBANK**, a *robust, parameter-free* calibration framework for restoring prompt-visual alignment on the fly. Instead of using static, pre-computed text embeddings, CONCEPTBANK constructs a dataset-specific dictionary, a concept bank, directly derived from the target domain’s statistics (specifically, the support set of  $\mathcal{D}$ ). This bank acts as a dynamic interface between SAM3’s frozen knowledge and the specific nuances of the deployment environment. CONCEPTBANK operates via three synergistic mechanisms: (*i*) it estimates class-wise *visual prototypes* to anchor concepts in the target feature space; (*ii*) it applies *representative support mining* to reduce the influence of outliers under severe drift, aligning with robust-estimation principles; and (*iii*) it performs *concept fusion* to synthesize calibrated query embeddings that better match

the target labeling semantics. Crucially, CONCEPTBANK requires no gradient updates to SAM3. It functions as a plug-and-play module that strengthens a generic OVS model for distribution-shifted deployment. We demonstrate that this approach is not only conceptually well-motivated but also empirically effective, improving robustness from standard natural-scene benchmarks to remote-sensing imagery. Our main contributions are summarized as follows:

- A drift-centric view of prompt-conditioned OVS is developed by separating *data drift* from *concept drift*, clarifying why static prompts fail under cross-domain use.
- We propose CONCEPTBANK, a *parameter-free* framework tailored for SAM3 that efficiently builds a dataset-specific concept bank from target support statistics.
- We introduce a three-stage construction pipeline comprising *prototype estimation*, *representative support mining*, and *prototype-consistent concept fusion* to stabilize calibration under appearance shifts and semantic relabeling.
- Extensive experiments on *natural-scene* and *remote-sensing* benchmarks show consistent gains over vanilla prompting and competitive performance against strong baselines in the presence of realistic distribution drift.

## 2. Method

### 2.1. Problem Formulation: Distribution Drift in OVS

Open-vocabulary segmentation is considered on a labeled target-domain dataset  $\mathcal{D} = \{(x_i, y_i)\}_{i=1}^N$  with  $N$  samples, where  $x_i \in \mathcal{X}$  denotes an image and  $y_i \in \{0, 1\}^{H \times W \times |\mathcal{C}|}$  is the corresponding set of category masks at spatial resolution  $H \times W$  for  $\mathcal{C}$ . The category set  $\mathcal{C}$  is specified at inference time via language prompts (or concept queries), and the model is expected to generalize beyond the pre-training vocabulary. The samples are assumed to be drawn from an underlying target distribution  $P_{\mathcal{D}}$ .

A pre-trained and frozen foundation model  $\Phi$  (instantiated by SAM3) is adopted, consisting of a visual encoder  $\phi_V : \mathcal{X} \rightarrow \mathbb{R}^d$  and a text encoder  $\phi_T : \mathcal{T} \rightarrow \mathbb{R}^d$ . Such models follow a *match-and-segment* paradigm: given a prompt  $t_c$  (*e.g.*, “a photo of a [class]”), a query embedding  $e_c = \phi_T(t_c)$  conditions the mask predictor to produce a binary segmentation  $\hat{y}^c$ . This inference process is summarized as:

$$\hat{y}^c = f_{\Phi}(x, e_c), \quad c \in \mathcal{C}. \quad (1)$$

The key obstacle in transferring  $\Phi$  from its pre-training environment  $\mathcal{S}$  to the target domain is the misalignment between target visual evidence and source-induced language anchors. This paper characterizes the deployment difficulty as a *dual-drift* phenomenon, including *data drift* ( $P_S(X) \neq P_{\mathcal{D}}(X)$ ) and *concept drift* ( $P_S(Y|X) \neq P_{\mathcal{D}}(Y|X)$ ). Both forms of drift manifest as degraded cross-modal alignment, thereby reducing the reliability of prompt-conditioned masks.

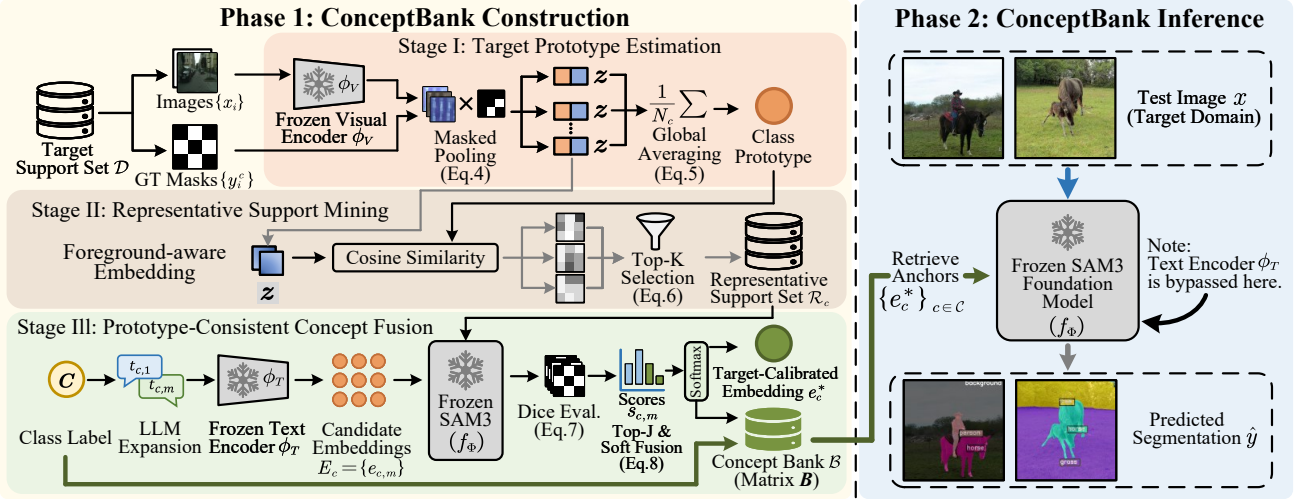


**Figure 2. Illustration of the proposed CONCEPTBANK framework.** **Phase 1 (Construction §2.2)** on target support set  $\mathcal{D}$ : **Stage I** estimates class prototypes using frozen  $\phi_V$  (masked pooling + class averaging); **Stage II** mines representative supports  $\mathcal{R}_c$  via cosine  $\text{Top}_K$ ; **Stage III** fuses LLM-expanded texts with visual guidance to produce target-calibrated embeddings  $e_c^*$ , forming Concept Bank  $\mathcal{B}$ . **Phase 2 (Inference §2.3)** on target test set: plug  $\mathcal{B}$  into frozen SAM3 for test segmentation, bypassing the text encoder  $\phi_T$ .

**Data Drift.** The marginal distribution of visual appearances shifts across domains (*e.g.*, sensor characteristics, spectral responses, viewpoints, illumination, and background context). Even when the semantic definition of class  $c$  remains unchanged, the target visual representations  $\phi_V(x)$  may move away from the source-induced query embedding  $e_c^S$  in the shared space, leading to weakened alignment:

$$P_S(X) \neq P_{\mathcal{D}}(X) \Rightarrow \mathbb{E}_{x \sim P_{\mathcal{D}}(X)}[\cos(\phi_V(x), e_c^S)] \downarrow. \quad (2)$$

**Concept Drift.** The conditional semantics of labels evolve across domains: the visual cues that support label  $c$  in  $\mathcal{S}$  may differ from those in  $\mathcal{D}$ . Consequently, a generic prompt embedding  $e_c^S$  can encode attributes that are irrelevant, ambiguous, or even contradictory under the target labeling rule, yielding a mis-specified language anchor:

$$P_S(Y|X) \neq P_{\mathcal{D}}(Y|X) \Rightarrow e_c^* \neq e_c^S. \quad (3)$$

In this work, our goal is to construct a concept bank  $\mathcal{B} = \{(c, e_c^*)\}_{c \in \mathcal{C}}$  that stores *target-calibrated* query embeddings. Under a fully frozen  $\Phi$ , the problem reduces to selecting, for each class  $c$ , a query embedding  $e_c^*$  that minimizes the target-domain segmentation risk induced by  $f_\Phi(\cdot, e_c)$  on the target-domain dataset  $\mathcal{D}$ , thereby restoring cross-modal alignment without any parameter update.

## 2.2. CONCEPTBANK: Construction

The construction of CONCEPTBANK is a one-time, offline process performed on the support set (training split) of the target dataset. It follows a three-stage pipeline that progressively filters noise and realigns the modality gap.

**Stage I: Prototype Estimation.** To alleviate data drift, we first need to understand where the target visual features lie

in the shared embedding space. Relying on global image pooling is insufficient for segmentation tasks as it introduces background noise. Instead, we employ *Mask-Pooled Crop Embeddings*. For a ground-truth mask  $y_i^c$  of class  $c$  in image  $x_i$ , we extract the specific object region  $v$ . Let  $\psi(u; v) \in \mathbb{R}^d$  be the dense visual feature at pixel location  $u$  within this crop. We compute the foreground-aware embedding  $z$ :

$$z(v, y_i^c) = \text{Norm}\left(\frac{\sum_u y_i^c(u) \cdot \psi(u; v)}{\sum_u y_i^c(u) + \epsilon}\right), \quad (4)$$

where  $\text{Norm}(\cdot)$  denotes  $\ell_2$  normalization and  $\epsilon$  is a stability constant (set to  $10^{-6}$  in this work). We then compute a global class prototype  $p_c$  by averaging these embeddings across all instances of class  $c$  in the support set:

$$p_c = \text{Norm}\left(\frac{1}{N_c} \sum_{i,v} z(v, y_i^c)\right), \quad (5)$$

where  $N_c$  denotes the number of available crops (instances) of class  $c$  in the support set. This prototype  $p_c$  serves as the empirical centroid of the target visual distribution.

**Stage II: Representative Support Mining.** Prototype estimation in **Stage I** provides a coarse target anchor  $p_c$ . However, directly calibrating language on the full set of crops  $\mathcal{V}_c$  is statistically fragile under severe drift. In practice,  $\mathcal{V}_c$  can contain (*i*) long-tail appearances induced by domain shift, (*ii*) heavy occlusions and truncations, (*iii*) background-dominated crops due to imperfect instance extraction, and (*iv*) annotation noise. Such atypical samples act as high-leverage points in high-dimensional embedding spaces, and can dominate any downstream calibration procedure, yielding a language anchor that explains outliers rather than the

target “core” (Huber, 2011; Rousseeuw & Hubert, 2011; Hampel, 1974). Let  $\mathcal{V}_c = \{(v, y)\}$  denote all available crops and their corresponding masks for class  $c$  in the support set. To obtain a stable and domain-representative evidence set, a *representative support set*  $\mathcal{R}_c$  is constructed by retaining only crops that are most consistent with the target prototype:

$$\mathcal{R}_c = \text{Top}_K(\mathcal{V}_c; (v, y) \mapsto \cos(\mathbf{z}(v, y), \mathbf{p}_c)), \quad (6)$$

where  $\mathbf{z}(v, y)$  is the mask-pooled crop embedding in Eq. (4). Here  $\text{Top}_K(\Omega; g)$  returns the subset of  $\Omega$  with the  $K$  largest scores under  $g$  (see Appendix A for the choice of  $K$ ). This step can be viewed as trimming the tail of the target embedding distribution and preserving a prototype-consistent core. Consequently, subsequent language calibration is conditioned on visually coherent, frequent target-domain evidence rather than being skewed by outliers under *data drift*.

**Stage III: Prototype-Consistent Concept Fusion.** Even with representative visual evidence, concept drift implies that the source-induced language anchor  $\mathbf{e}_c^S$  may not describe how class  $c$  is realized in the target domain. A key observation is that this failure mode is *functional*: two prompts with similar embedding similarity can yield markedly different masks. Therefore, prompt selection is formulated as choosing a query embedding that induces high-fidelity segmentation on the representative supports  $\mathcal{R}_c$ .

**Concept Pooling.** A pool of candidate prompts,  $\mathcal{T}_c = \{t_{c,1}, \dots, t_{c,M}\}$ , is generated by expanding each class name into diverse textual descriptions. Specifically, an off-the-shelf LLM (e.g., GPT) generates synonyms and attribute-enriched variants conditioned on the dataset documentation (e.g., the original paper and label taxonomy), grounding the candidates in the dataset’s label definitions. Crucially, this step is constrained to text-level rewriting and rephrasing of the provided descriptions, without introducing any new visual concepts, and thus serves purely as non-parametric prompt augmentation. More details and quality-control protocols are deferred to the Appendix A. Finally, the frozen text encoder maps each candidate to the shared space, yielding text prompt embeddings  $\mathbf{E}_c = \{\phi_T(t) \mid t \in \mathcal{T}_c\}$ .

**Concept Scoring.** Each candidate embedding  $\mathbf{e}_{c,m} \in \mathbf{E}_c$  is evaluated by the segmentation quality it induces on  $\mathcal{R}_c$ . The score  $s_{c,m}$  is defined as the average Dice coefficient over representative supports:

$$s_{c,m} = \frac{1}{|\mathcal{R}_c|} \sum_{(v,y) \in \mathcal{R}_c} \text{Dice}(f_\Phi(v, \mathbf{e}_{c,m}), y). \quad (7)$$

Instead of using cosine similarity as a static proxy, we propose a prototype-consistent metric that evaluates candidate concepts via the functional behavior of  $f_\Phi$  on target data. By grounding the ranking in the model’s operational context, our method effectively mitigates *concept drift*.

**Concept Fusion.** Relying on a single prompt is often unstable: different phrasings can lead to non-negligible performance variations even when they describe the same concept. Prompt ensembling has been widely used to mitigate such sensitivity by aggregating multiple semantically compatible prompts, improving robustness and generalization in vision-language transfer. Accordingly, an index set of high-scoring candidates is selected as  $\mathcal{J}_c = \text{Top}_J([M]; m \mapsto s_{c,m})$ , where  $[M] = \{1, \dots, M\}$ , and Appendix A details the choice of  $J$ . The final calibrated embedding  $\mathbf{e}_c^*$  is obtained by temperature-scaled soft fusion over  $\mathcal{J}_c$ :

$$\begin{aligned} \mathbf{e}_c^* &= \sum_{j \in \mathcal{J}_c} w_{c,j} \cdot \text{Norm}(\mathbf{e}_{c,j}), \\ w_{c,j} &= \frac{\exp(s_{c,j}/\tau)}{\sum_{k \in \mathcal{J}_c} \exp(s_{c,k}/\tau)}, \end{aligned} \quad (8)$$

where  $\tau$  controls the concentration of the mixture weights, serving as a standard smoothing mechanism for softmax-based aggregation (Hinton et al., 2015). This aggregation yields a calibrated language anchor that remains task-consistent while reducing prompt-level variance, and the resulting pairs  $(c, \mathbf{e}_c^*)$  constitute the concept bank  $\mathcal{B}$ .

### 2.3. CONCEPTBANK: Inference

Once the concept bank  $\mathcal{B} = \{(c, \mathbf{e}_c^*)\}_{c \in \mathcal{C}}$  is constructed on the target support set, inference in the target domain reduces to prompt-conditioned segmentation with target-calibrated query embeddings. During inference, the system retrieves  $\{\mathbf{e}_c^*\}_{c \in \mathcal{C}}$  from  $\mathcal{B}$  and uses them as language anchors for mask prediction. Each  $\mathbf{e}_c^*$  already aggregates multiple candidate descriptions through **Stage III**, so inference uses one consolidated embedding per class rather than multiple prompts. The text encoder  $\phi_T$  is unnecessary in this phase, and  $\mathcal{B}$  is stored as a compact embedding matrix  $\mathbf{B} \in \mathbb{R}^{|\mathcal{C}| \times d}$  with one row per class. Given an input image  $x$ , the inference model outputs masks via:

$$\hat{y} = f_\Phi(x, \{\mathbf{e}_c^*\}_{c \in \mathcal{C}}). \quad (9)$$

CONCEPTBANK keeps the match-and-segment paradigm  $f_\Phi$  intact and only replaces generic source-induced prompts with target-calibrated anchors from  $\mathcal{B}$ , yielding a plug-in correction for distribution drift without modifying  $\Phi$ .

In this work, our CONCEPTBANK is a *parameter-free* framework that adapts SAM3 for OVS: it never updates the parameters of  $\Phi$  and constructs  $\mathcal{B}$  via forward-only evaluation and non-parametric aggregation on the target support set. During inference, CONCEPTBANK remains strictly feed-forward with  $\Phi$  fully frozen. Since each  $\mathbf{e}_c^*$  consolidates multiple candidate descriptions offline and  $\phi_T$  is bypassed, the runtime cost matches a single-prompt pipeline and improves over multi-prompt ensembling baselines. No gradient-based updates or support samples are used during inference. The additional cost is storing  $\mathbf{B}$ , which scales linearly with  $|\mathcal{C}|$ .

Table 1. Quantitative comparison of OVS on natural-scene datasets. “Parameter-free” denotes methods without learnable parameters or gradient-based optimization. Metric values are mIoU (%). **bold** and underlined indicate the best and second-best results, respectively.

Method	Pub. & Year	Backbone (Size)	with background				without background				Avg.
			V21	PC60	COCO-O	V20	PC59	COCO-S	City	ADE	
<b>Training-based</b>											
GroupViT (Xu et al., 2022a)	CVPR’22	GroupViT (ViT-S/16)	50.4	18.7	27.5	79.7	23.4	15.3	11.1	9.2	29.4
TCL (Cha et al., 2023)	CVPR’23	CLIP	51.2	24.3	30.4	77.5	30.3	19.6	23.1	14.9	33.9
SegCLIP (Luo et al., 2023)	ICML’23	CLIP	52.6	24.7	27.5	-	-	-	-	-	-
CoDe (Wu et al., 2024)	CVPR’24	CLIP	57.7	30.5	32.3	-	-	23.9	28.9	17.7	-
SAM-CLIP (Wang et al., 2024b)	CVPR’24	CLIP + SAM (ViT-B/16)	60.6	29.2	-	-	-	31.5	-	17.1	-
CLIP-DINOiser (Wysoczanska et al., 2024)	ECCV’24	CLIP + DINO (ViT-B/16)	62.1	32.4	34.8	80.9	35.9	24.6	31.7	20.0	40.3
Talk2DINO (Barsellotti et al., 2025)	ICCV’25	CLIP + DINOv2 <sup>†</sup> (ViT-B/14)	65.8	37.7	45.1	88.5	42.4	30.2	38.1	22.5	46.3
<b>Parameter-free</b>											
CLIP (Radford et al., 2021)	ICML’21	CLIP	18.6	7.8	6.5	49.1	11.2	7.2	6.7	3.2	13.8
FreeDA (Barsellotti et al., 2024)	CVPR’24	CLIP + DINOv2 (ViT-B/14)	51.8	35.3	36.3	84.3	39.7	25.7	34.1	20.8	41.0
GEM (Bousselham et al., 2024)	CVPR’24	CLIP	46.2	-	-	-	32.6	15.7	-	-	-
CaR (Sun et al., 2024)	CVPR’24	CLIP	48.6	13.6	15.4	73.7	18.4	-	-	5.4	-
LaVG (Kang & Cho, 2024)	ECCV’24	CLIP + DINO (ViT-B/8)	62.1	31.6	34.2	82.5	34.7	23.2	26.2	15.8	38.8
ProxyCLIP (Lan et al., 2024a)	ECCV’24	CLIP + DINOv2 <sup>†</sup> (ViT-B/14)	58.6	33.8	37.4	83.0	37.2	25.4	33.9	19.7	41.1
CLIPTrase (Shao et al., 2024)	ECCV’24	CLIP	50.9	29.9	43.6	81.0	33.8	22.8	21.3	16.4	32.7
ClearCLIP (Lan et al., 2024b)	ECCV’24	CLIP	51.8	32.6	33.0	80.9	35.9	23.9	30.0	16.7	38.1
SCLIP* (Wang et al., 2024a)	ECCV’24	CLIP	59.1	30.4	30.5	80.4	34.1	22.4	32.2	16.1	38.2
NACLIP* (Hajimiri et al., 2025)	WACV’25	CLIP	58.9	32.2	33.2	79.7	35.2	23.3	35.5	17.4	39.4
LPOSS (Stojnić et al., 2025)	CVPR’25	CLIP + DINO (ViT-B/16)	61.1	34.6	33.4	78.8	37.8	25.9	37.3	21.8	41.3
CASS* (Kim et al., 2025)	CVPR’25	CLIP + DINO (ViT-B/8)	65.8	36.7	37.8	87.8	40.2	26.7	39.4	20.4	44.4
$\mathcal{DTH}$ -CLIP (Duan et al., 2025)	ICCV’25	CLIP	64.2	36.0	37.4	84.9	39.7	26.7	40.2	19.6	43.6
SFP (Jin et al., 2025) (Jin et al., 2025)	ICCV’25	CLIP	63.9	37.2	37.9	84.5	39.9	26.4	41.1	20.8	44.0
CorrCLIP (Zhang et al., 2025)	ICCV’25	CLIP (ViT-L/14) + DINO (ViT-B/8) + SAM2 (Hiera-L)	76.7	44.9	49.4	91.5	50.8	34.0	51.1	30.7	53.6
Trident (Shi et al., 2025)	ICCV’25	CLIP + DINO (ViT-B/16) + SAM (ViT-B/16)	67.1	38.6	41.1	84.5	42.2	28.3	42.9	21.9	45.8
ReME (Xuan et al., 2025)	ICCV’25	CLIP + DINOv2 (ViT-L/14) + SAM (ViT-L/16)	82.2	44.6	48.2	93.2	53.1	33.3	59.0	28.2	55.2
RF-CLIP (Li et al., 2026b)	AAAI’26	CLIP	67.2	37.9	39.1	87.0	41.4	27.5	43.0	21.0	45.5
SAM3* (Carion et al., 2026)	ICLR’26	SAM3 (PE-L+/14)	81.9	46.1	65.4	88.9	50.0	33.3	62.3	31.8	57.5
<b>CONCEPTBANK (Ours)</b>	-	SAM3 (PE-L+/14)	<b>87.1</b>	<b>56.5</b>	<b>67.9</b>	<b>97.4</b>	<b>63.0</b>	<b>46.4</b>	<b>75.1</b>	<b>43.3</b>	<b>67.1</b>

Notes: Unless otherwise specified, CLIP uses ViT-B/16 (Dosovitskiy et al., 2021). “\*” denotes results reproduced in our work. “†” indicates DINOv2 equipped with registers (Darce et al., 2024). “-” indicates results are not reported or applicable in the original paper.

### 3. Experiments

#### 3.1. Experimental Setup

**Datasets.** Experiments follow the standard OVS setting on eight natural-scene datasets, including protocols *with* and *without* a background category. The *with-background* subset includes Pascal VOC 21 (V21, 21 classes) (Everingham et al., 2015), Pascal Context 60 (PC60, 60 classes) (Mottaghi et al., 2014), and COCO-Object (COCO-O, 80 object classes from MS-COCO) (Lin et al., 2014). The *without-background* subset includes Pascal VOC 20 (V20, 20 classes) (Everingham et al., 2015), Pascal Context 59 (PC59, 59 classes) (Mottaghi et al., 2014), COCO-Stuff (COCO-S, 171 classes) (Caesar et al., 2018), Cityscapes (City, 19 classes) (Cordts et al., 2016), and ADE20K (ADE, 150 classes) (Zhou et al., 2017). Unless stated otherwise, results are reported on the official validation splits using the public class-name lists. To probe distribution drift in OVS beyond natural-scene imagery, experiments additionally include four remote-sensing datasets, each with an explicit background class: LoveDA (7 classes) (Wang et al., 2021), Potsdam (ISPRS, 2012a) (6 classes), Vaihingen (ISPRS, 2012b) (6 classes), and iSAID (16 classes) (Waqas Zamir et al., 2019). These aerial benchmarks exhibit pronounced shifts in acquisition conditions and visual statistics (e.g.,

viewpoint, scale, and sensor characteristics), offering a challenging evaluation setting for distribution drift in OVS.

**Implementation and Evaluation Details.** All experiments use the official SAM3 (Carion et al., 2026) model with the PE-L+ (Bolya et al., 2025) backbone and the default configuration, while keeping  $\Phi$  fully frozen. Inputs are resized to  $1008 \times 1008$ , matching the native SAM3 resolution. Unlike CLIP-style OVS pipelines, generic prompt templates (e.g., “a photo of a [class]”) are not used. Category names serve as the base prompts. For concept bank construction, we use GPT to generate synonyms and attribute-enriched descriptions for each class conditioned on the dataset’s original paper and label definitions. The prompts used for this generation are provided in the Appendix D, and we restrict the generation to text-level rewriting without introducing new visual concepts (cf. §2.2-*Stage III*). During inference, each class uses a single calibrated embedding  $e_c^*$  from  $\mathcal{B}$  and bypasses the text encoder  $\phi_T$ . All results are single-scale, without test-time augmentation, multi-scale or flip evaluation, and without post-processing or refinement (e.g., DenseCRF (Krähenbühl & Koltun, 2011) or PAMR (Araslanov & Roth, 2020)). All experiments are run on four NVIDIA V100 GPUs (32 GB). Following prior works (Wang et al., 2024a; Hajimiri et al., 2025; Lan et al., 2024a), performance is measured by mean Intersection-over-Union (**mIoU**).

Table 2. Quantitative comparison of OVS on remote-sensing datasets. “Parameter-free” denotes methods without learnable parameters or gradient-based optimization. Metric values are mIoU (%). **bold** and underlined indicate the best and second-best results, respectively.

Method	Pub. & Year	Backbone (Size)	with background				Avg.
			LoveDA	Potsdam	Vaihingen	iSAID	
<b>Training-based</b>							
SAN (Xu et al., 2023)	CVPR’23	CLIP (ViT-L/14@336px)	25.3	37.3	39.2	<u>49.6</u>	37.9
Cat-Seg (Cho et al., 2024)	CVPR’24	CLIP (ViT-L/14@336px)	28.6	35.8	42.3	<u>53.3</u>	40.0
SkySense-O (Zhu et al., 2025)	CVPR’25	CLIP (ViT-L/14@512px)	<u>38.3</u>	<u>54.1</u>	<u>51.6</u>	43.9	<u>47.0</u>
RSKT-Seg (Li et al., 2026a)	AAAI’26	CLIP (ViT-L/14@336px) + RemoteCLIP <sup>†</sup> (ViT-B/16) + DINO (ViT-B/32)	33.2	38.4	42.7	<u>54.3</u>	42.2
<b>Parameter-free</b>							
CLIP (Radford et al., 2021)	ICML’21	CLIP	12.4	15.6	10.8	7.5	11.6
MaskCLIP (Zhou et al., 2022a)	ECCV’22	CLIP	27.8	33.9	29.9	14.5	26.5
GEM (Bousselham et al., 2024)	CVPR’24	CLIP	31.6	39.1	36.4	17.7	31.2
ProxyCLIP (Lan et al., 2024a)	ECCV’24	CLIP + DINOv2 <sup>†</sup> (ViT-B/14)	34.3	49.0	47.5	21.8	38.2
SCLIP* (Wang et al., 2024a)	ECCV’24	CLIP	30.4	39.6	35.9	16.1	30.5
SegEarth-OV* (Li et al., 2025a)	CVPR’25	CLIP	36.9	48.5	40.0	21.7	36.8
CorrCLIP* (Zhang et al., 2025)	ICCV’25	CLIP + DINO (ViT-B/8) + SAM2 (Hiera-L)	36.9	51.9	47.0	25.5	40.3
SAM3* (Carion et al., 2026)	ICLR’26	SAM3 (PE-L/14)	35.6	<u>54.1</u>	49.1	17.7	39.1
<b>CONCEPTBANK (Ours)</b>	-	SAM3 (PE-L/14)	<b>49.4</b>	<b>60.5</b>	<b>63.0</b>	35.4	<b>52.1</b>

Notes: Unless otherwise specified, CLIP uses ViT-B/16 (Dosovitskiy et al., 2021). “\*” denotes results reproduced in our work. “†” indicates DINOv2 equipped with registers. “‡” indicates RemoteCLIP (Liu et al., 2024), a CLIP-based remote sensing foundation model.

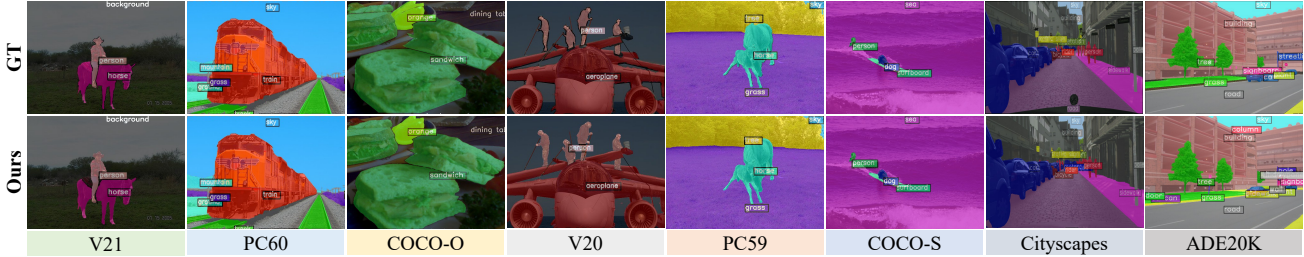


Figure 3. Qualitative comparison results of open-vocabulary segmentation on natural-scene datasets. Zoom in for best view.

### 3.2. Comparison with State-of-the-Arts

**Quantitative Results (Natural-Scene).** Table 1 reports results on eight natural-scene benchmarks under the OVS protocol. Most existing methods rely on CLIP-based representations, either through direct prompt matching or by pairing CLIP with auxiliary vision backbones (e.g., DINO/SAM). SAM3 serves as a particularly strong baseline. Even without calibration, it surpasses all CLIP-based pipelines on average (57.5 mIoU) and rivals the strongest parameter-heavy methods, such as ReME (Xuan et al., 2025), highlighting the advantage of promptable mask decoding backed by a strong visual foundation. However, SAM3 is not fully “wild-ready”: on taxonomy- and context-heavy datasets (e.g., PC60, PC59, and ADE), generic source-induced prompts still misalign with target-domain semantics due to distribution drift, leaving substantial headroom. CONCEPTBANK directly bridges this gap by replacing generic prompts with target-calibrated anchors stored in a concept bank. Building on the same frozen SAM3, CONCEPTBANK improves performance across all datasets, achieving the best overall average of **67.1** mIoU. The largest gains appear on PC60 (**+10.4**), PC59 (**+13.0**), and City (**+12.8**), suggesting that these datasets are most susceptible to distribution-drift effects on prompt-conditioned masks. Since CONCEPTBANK introduces no architectural changes or parameter updates to  $\Phi$ , these improvements are attributed solely to concept-level

calibration, effectively taming SAM3 for OVS in the wild.

**Quantitative Results (Remote-Sensing).** Table 2 presents results on four remote-sensing benchmarks, where distribution drift is more severe due to acquisition and scale differences. CLIP-based pipelines remain the dominant paradigm, and even training-based remote-sensing methods or CLIP variants augmented with additional backbones show limited transferability across datasets. In this regime, SAM3 again provides a strong starting point, achieving an average mIoU of 39.1 and already outperforming most CLIP-based baselines. Yet, it still shows clear room for improvement on drift-heavy categories and scenes (notably LoveDA and iSAID). CONCEPTBANK consistently strengthens SAM3 under these drifts. Built on the same frozen backbone and decoder, CONCEPTBANK attains the best average of **52.1** mIoU, improving over SAM3 by **+13.0** on average. The performance gains are substantial on all datasets, including LoveDA (**+13.8**), Potsdam (**+6.4**), Vaihingen (**+13.9**), and iSAID (**+17.7**). Consequently, our CONCEPTBANK achieves the best performance on three out of four benchmarks while remaining clearly ahead on the overall average. These quantitative results substantiate the indispensability of concept bank calibration for remote-sensing open-vocabulary segmentation, specifically for counteracting semantic misalignment between source prompts and bridging the severe distributional drift from natural pre-training data.

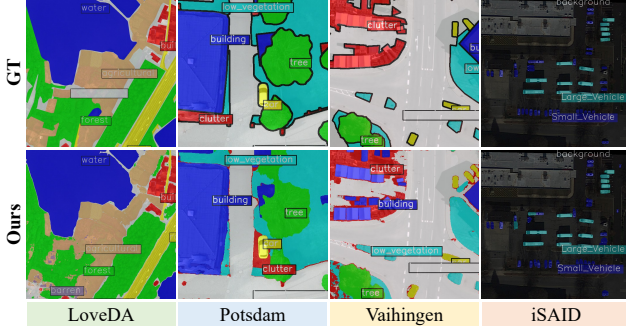


Figure 4. Qualitative comparison results of open-vocabulary segmentation on remote-sensing datasets. Zoom in for best view.

Table 3. Component analysis of CONCEPTBANK (cf. §2.2). NS and RS denote Natural-Scene and Remote-Sensing benchmarks.

Variant	Stage			Avg. mIoU	
	I	II	III	NS	RS
Vanilla SAM3 (classname only)				57.5	39.1
+ Prompt Expansion				58.0 $\Delta 0.5$	42.2 $\Delta 3.1$
+ Prototype Anchoring	✓			60.1 $\Delta 2.6$	45.5 $\Delta 6.4$
+ Representative Mining	✓	✓		62.8 $\Delta 5.3$	48.2 $\Delta 9.1$
<b>CONCEPTBANK (Full)</b>	✓	✓	✓	<b>64.7 <math>\Delta 7.2</math></b>	<b>52.1 <math>\Delta 13.0</math></b>

**Qualitative Results.** As shown in Fig. 3, CONCEPTBANK predictions align closely with GT masks across eight natural-scene benchmarks with diverse taxonomies. The masks essentially preserve scene-level layout and class extents, with most deviations concentrated on fine structures and ambiguous boundaries. Fig. 4 further illustrates CONCEPTBANK on four remote-sensing datasets, whose overhead viewpoints and scale patterns differ markedly from natural scenes. Our method still produces coherent large-area land-cover and man-made regions, while remaining errors mostly occur on small objects, thin boundaries, and cluttered areas where visually similar classes are challenging to separate. Overall, these qualitative results support CONCEPTBANK as a concept-level calibration framework that improves prompt-conditioned masks without modifying the frozen SAM3.

### 3.3. Ablation Study

This section analyzes the proposed CONCEPTBANK to isolate the effect of each design choice. All ablations follow the protocol in §3.1 with SAM3 kept frozen and identical data splits, and additional ablations are deferred to the *Supplementary Material* (§A) due to space constraints.

**Component Analysis.** Table 3 isolates the contribution of each stage in CONCEPTBANK by progressively enabling Stages I-III. A plain SAM3 baseline already performs strongly on NS (57.5), yet drops on RS (39.1), reflecting the larger distribution drift. Naive prompt expansion without fusion brings only marginal improvement on NS (+0.5) but a clearer gain on RS (+3.1), suggesting that richer descriptions help but do not resolve misalignment by themselves. Adding

Table 4. Ablation on prompt expansion strategies. NS and RS denote Natural-Scene and Remote-Sensing benchmarks.

Variant	Prompt	Avg. mIoU	
	Source	NS	RS
Vanilla SAM3 (classname only)	-	57.5	39.1
+ Prompt Expansion	Gemini-3 Pro	57.8 $\Delta 0.3$	42.1 $\Delta 3.0$
CONCEPTBANK	Gemini-3 Pro	64.3 $\Delta 6.8$	51.8 $\Delta 12.7$
+ Prompt Expansion	GPT-5.2	58.0 $\Delta 0.5$	42.2 $\Delta 3.1$
CONCEPTBANK	GPT-5.2	<b>64.7 <math>\Delta 7.2</math></b>	<b>52.1 <math>\Delta 13.0</math></b>

Table 5. Inference efficiency comparison. Relative FPS measures inference speed normalized to the single-prompt SAM3 baseline.

Variant	Text Encoder	Relative FPS
Vanilla SAM3 (classname only)	On-the-fly	1.00 $\times$
Vanilla SAM3 (prompt expansion)	On-the-fly	0.18 $\times$
<b>CONCEPTBANK</b>	Bypassed	<b>1.25<math>\times</math></b>

Stage I yields a larger and consistent boost, especially on RS (+6.4), indicating that grounding concepts in target visual statistics is critical under appearance drift. Stage II further improves both settings (NS: +5.3, RS: +9.1), supporting its role in filtering atypical or low-quality supports that destabilize calibration. Finally, Stage III provides an additional gain and delivers the best overall averages (NS: 64.7, RS: 52.1), showing that consolidating high-scoring candidates into a single calibrated anchor is necessary to fully exploit the expanded concept pool. Overall, each stage contributes non-trivially, and the full pipeline achieves the most stable improvements across both benchmark families.

**Effect of Prompt Expansion and LLM Choice.** Table 4 reports prompt expansion and then evaluates it under CONCEPTBANK. Prompt expansion alone is modest on Natural-Scene benchmarks (+0.3 with Gemini-3 Pro, +0.5 with GPT-5.2) and more noticeable on Remote-Sensing (+3.0/+3.1), but it remains far from closing the gap induced by drift. Once the same candidates are calibrated by CONCEPTBANK, performance rises sharply to **64.3/51.8** (Gemini-3 Pro) and **64.7/52.1** (GPT-5.2), *i.e.*, +6.8/+12.7 and +7.2/+13.0 over vanilla SAM3. Equivalently, CONCEPTBANK contributes an additional +6.5/+9.7 (Gemini-3 Pro) and +6.7/+9.9 (GPT-5.2) beyond prompt expansion, showing that the gains come from target-conditioned calibration rather than from richer text alone. The same pattern holds for both LLMs, indicating that our CONCEPTBANK is robust to the choice of generator, with GPT-5.2 giving a small but consistent edge.

**Inference Efficiency.** Table 5 summarizes runtime throughput *during inference only*. We report relative FPS for the online segmentation pipeline and exclude Concept Bank construction, which is a one-time offline cost discussed in the Appendix B. Vanilla SAM3 with a single class-name prompt sets the reference (1.00 $\times$ ), whereas evaluating multiple prompts per class slows inference sharply (0.18 $\times$ ) due to repeated text encoding and per-prompt mask decoding. In

contrast, CONCEPTBANK retrieves pre-calibrated anchors from  $\mathcal{B}$  and bypasses the text encoder entirely, so each class uses one consolidated embedding at runtime. This keeps the online procedure close to the single-prompt baseline and yields a modest speedup in practice ( $1.25\times$ ), while maintaining the same frozen  $\Phi$  and decoding path.

## 4. Related Work

**Open-Vocabulary Segmentation and Foundation Models.** Semantic segmentation has been historically studied in a closed-set regime with fully supervised architectures such as FCN (Long et al., 2015), DeepLab (Chen et al., 2017), and Transformer-based designs (Xie et al., 2021), evaluated on curated benchmarks (*e.g.*, PASCAL VOC, MS-COCO, ADE20K, Cityscapes, COCO-Stuff). Moving beyond fixed taxonomies motivates open-vocabulary formulations, where early zero-shot transfer leveraged semantic embeddings and class descriptions (Zhao et al., 2017; Bucher et al., 2019). The modern surge is driven by vision-language models such as CLIP (Radford et al., 2021), ALIGN (Jia et al., 2021), and EVA (Fang et al., 2023), together with prompt design/learning strategies that improve text conditioning in downstream tasks (Zhou et al., 2022b; Khattak et al., 2023; Zhang et al., 2022; Pratt et al., 2023). In parallel, unified decoders and multi-task segmentation frameworks broaden the interface for language-conditioned dense prediction (Zou et al., 2023a;b; Li et al., 2022a; Ghiasi et al., 2022; Li et al., 2022b; Zhong et al., 2022; Zhou et al., 2022c). Segment-anything style foundation models inject strong mask priors and promptable decoding into segmentation pipelines (Kirillov et al., 2023; Ravi et al., 2025; Carion et al., 2026), and hybrid systems further couple these priors with VLM embeddings for semantic grounding (Wang et al., 2024b). A recurring bottleneck, however, is that cross-modal alignment learned on pre-training environments can degrade under distribution drift, a phenomenon well documented in concept-drift and data-drift literature (Gama et al., 2014; Lu et al., 2018; Kore et al., 2024). This work addresses the same open-vocabulary interface but targets drift explicitly via a parameter-free concept bank that calibrates language anchors to target evidence while keeping  $\Phi$  fully frozen.

**Training-Based and Parameter-Free OVS under Distribution Drift.** Training-based OVS methods adapt VLMs to dense prediction by learning mask-aware objectives, decoders, or adapters on additional data (Xu et al., 2022b; Mukhoti et al., 2023; Luo et al., 2023; Cho et al., 2024; Xu et al., 2022a). Another strong direction fuses complementary foundations, *e.g.*, self-supervised ViTs (Caron et al., 2021; Oquab et al., 2023; Siméoni et al., 2025; Wang et al., 2022; Simeoni et al., 2023; Wang et al., 2023) and diffusion priors (Rombach et al., 2022; Karazija et al., 2024), to refine localization and objectness, often with distillation-style transfers (Hinton et al., 2015; Wysoczanska et al., 2024; Jose

et al., 2025; Barsellotti et al., 2025). In contrast, parameter-free OVS keeps backbones frozen and improves inference by reweighting attention, reconstructing patch correlations, suppressing outliers, or enforcing spatial coherence (Zhou et al., 2022a; Lan et al., 2024a; Wang et al., 2024a; Hajimiri et al., 2025; Kim et al., 2025; Zhang et al., 2025; Kang et al., 2025; Xuan et al., 2025). These approaches can be effective but remain sensitive to drift because prompt semantics and visual evidence can become mismatched across domains (Tu et al., 2023; Gama et al., 2014; Lu et al., 2018; Kore et al., 2024). The issue is amplified in remote sensing, where sensor characteristics and viewing geometry induce large appearance shifts. Recent work, therefore, adapts OVS pipelines to aerial benchmarks using either training-based or foundation-model-heavy designs (Liu et al., 2024; Li et al., 2025a; Zhu et al., 2025; Li et al., 2026a). Robust estimation principles also emphasize the disproportionate impact of high-leverage outliers in high-dimensional settings, aligning with the need for representative evidence selection before any calibration. In this context, CONCEPTBANK departs from heuristic prompt ensembling by constructing a dataset-specific concept bank through prototype anchoring, representative support mining, and task-conditioned concept fusion, thereby strengthening SAM3 for open-vocabulary segmentation under realistic distribution drift.

## 5. Conclusion

This work studies why promptable open-vocabulary segmentation with SAM3 degrades under distribution drift and presents CONCEPTBANK, a parameter-free calibration framework that restores prompt-mask alignment through a dataset-specific concept bank. CONCEPTBANK keeps the match-and-segment operator  $f_\Phi$  intact and calibrates only the language anchors using target-domain statistics. It estimates class-wise visual prototypes to anchor target evidence, mines representative supports to reduce the influence of outliers induced by data drift, and fuses candidate concepts to correct mis-specified prompts resulting from concept drift. Across natural-scene and remote-sensing benchmarks, CONCEPTBANK consistently strengthens SAM3’s open-vocabulary segmentation, demonstrating that concept-level calibration is an effective and practical route to taming foundation segmentation models in the wild.

**Limitation and Future Work.** Most current OVS methods remain constrained by fixed label taxonomies and static text prompts. When class definitions are ambiguous, overlapping, or evolve across datasets, the boundary between concept drift and annotation inconsistency becomes ill-posed, and even a calibrated concept bank cannot fully resolve inherently subjective labeling rules. We aim to generalize this concept-level calibration strategy to other multi-modal foundation models beyond segmentation.

## Impact Statement

This paper presents work whose goal is to enhance the robustness and adaptability of open-vocabulary segmentation. There are many potential societal consequences of our work, none which we feel must be specifically highlighted here.

## References

Araslanov, N. and Roth, S. Single-stage semantic segmentation from image labels. In *CVPR*, pp. 4253–4262, 2020.

Barsellotti, L., Amoroso, R., Cornia, M., Baraldi, L., and Cucchiara, R. Training-free open-vocabulary segmentation with offline diffusion-augmented prototype generation. In *CVPR*, pp. 3689–3698, 2024.

Barsellotti, L., Bianchi, L., Messina, N., Carrara, F., Cornia, M., Baraldi, L., Falchi, F., and Cucchiara, R. Talking to dino: Bridging self-supervised vision backbones with language for open-vocabulary segmentation. In *ICCV*, pp. 22025–22035, 2025.

Bolya, D., Huang, P.-Y., Sun, P., Cho, J. H., Madotto, A., Wei, C., Ma, T., Zhi, J., Rajasegaran, J., Rasheed, H., et al. Perception encoder: The best visual embeddings are not at the output of the network. *arXiv preprint arXiv:2504.13181*, 2025.

Bousselham, W., Petersen, F., Ferrari, V., and Kuehne, H. Grounding everything: Emerging localization properties in vision-language transformers. In *CVPR*, pp. 3828–3837, 2024.

Bucher, M., Vu, T.-H., Cord, M., and Perez, P. Zero-shot semantic segmentation. In *NeurIPS*, pp. 469–479, 2019.

Caesar, H., Uijlings, J., and Ferrari, V. COCO-Stuff: Thing and stuff classes in context. In *CVPR*, pp. 1209–1218, 2018.

Carion, N., Gustafson, L., Hu, Y.-T., Debnath, S., Hu, R., Suris, D., Ryali, C., Alwala, K. V., Khedr, H., Huang, A., et al. Sam 3: Segment anything with concepts. In *ICLR*, 2026.

Caron, M., Touvron, H., Misra, I., Jégou, H., Mairal, J., Bojanowski, P., and Joulin, A. Emerging properties in self-supervised vision transformers. In *ICCV*, pp. 9650–9660, 2021.

Cha, J., Mun, J., and Roh, B. Learning to generate text-grounded mask for open-world semantic segmentation from only image-text pairs. In *CVPR*, pp. 11165–11174, 2023.

Chen, L.-C., Papandreou, G., Kokkinos, I., Murphy, K., and Yuille, A. L. Deeplab: Semantic image segmentation with deep convolutional nets, atrous convolution, and fully connected crfs. *TPAMI*, 40(4):834–848, 2017.

Cho, S., Shin, H., Hong, S., Arnab, A., Seo, P. H., and Kim, S. Cat-seg: Cost aggregation for open-vocabulary semantic segmentation. In *CVPR*, pp. 4113–4123, 2024.

Cordts, M., Omran, M., Ramos, S., Rehfeld, T., Enzweiler, M., Benenson, R., Franke, U., Roth, S., and Schiele, B. The cityscapes dataset for semantic urban scene understanding. In *CVPR*, pp. 3213–3223, 2016.

Darcet, T., Oquab, M., Mairal, J., and Bojanowski, P. Vision transformers need registers. In *ICLR*, 2024.

Dosovitskiy, A., Beyer, L., Kolesnikov, A., Weissenborn, D., Zhai, X., Unterthiner, T., Dehghani, M., Minderer, M., Heigold, G., Gelly, S., Uszkoreit, J., and Houlsby, N. An image is worth 16x16 words: Transformers for image recognition at scale. In *ICLR*, 2021.

Duan, S., Yang, X., and Wang, N. Dih-clip: Unleashing the diversity of multi-head self-attention for training-free open-vocabulary semantic segmentation. In *ICCV*, pp. 22794–22803, 2025.

Everingham, M., Eslami, S. A., Van Gool, L., Williams, C. K., Winn, J., and Zisserman, A. The pascal visual object classes challenge: A retrospective. *IJCV*, 111(1): 98–136, 2015.

Fang, Y., Wang, W., Xie, B., Sun, Q., Wu, L., Wang, X., Huang, T., Wang, X., and Cao, Y. EVA: Exploring the limits of masked visual representation learning at scale. In *CVPR*, pp. 19358–19369, 2023.

Gama, J., Žliobaitė, I., Bifet, A., Pechenizkiy, M., and Bouchachia, A. A survey on concept drift adaptation. *CSUR*, 46(4):1–37, 2014.

Ghiasi, G., Gu, X., Cui, Y., and Lin, T.-Y. Scaling open-vocabulary image segmentation with image-level labels. In *ECCV*, pp. 540–557, 2022.

Hajimiri, S., Ayed, I. B., and Dolz, J. Pay attention to your neighbours: Training-free open-vocabulary semantic segmentation. In *WACV*, pp. 5061–5071, 2025.

Hampel, F. R. The influence curve and its role in robust estimation. *Journal of the American Statistical Association*, 69(346):383–393, 1974.

Hinton, G., Vinyals, O., and Dean, J. Distilling the knowledge in a neural network. *arXiv preprint arXiv:1503.02531*, 2015.

Huber, P. J. Robust statistics. In *International Encyclopedia of Statistical Science*, pp. 1248–1251. Springer, 2011.

ISPRS. ISPRS 2D Semantic Labeling Challenge - Potsdam. <https://www.isprs.org/resources/datasets/benchmarks/UrbanSemLab/2d-sem-label-potsdam.aspx>, 2012a.

ISPRS. ISPRS 2D Semantic Labeling Challenge - Vaihingen. <https://www.isprs.org/resources/datasets/benchmarks/UrbanSemLab/2d-sem-label-vaihingen.aspx>, 2012b.

Jia, C., Yang, Y., Xia, Y., Chen, Y.-T., Parekh, Z., Pham, H., Le, Q., Sung, Y.-H., Li, Z., and Duerig, T. Scaling up visual and vision-language representation learning with noisy text supervision. In *ICML*, pp. 4904–4916, 2021.

Jin, S., Yu, S., Zhang, B., Sun, M., Dong, Y., and Xiao, J. Feature purification matters: Suppressing outlier propagation for training-free open-vocabulary semantic segmentation. In *ICCV*, pp. 20291–20300, 2025.

Jose, C., Moutakanni, T., Kang, D., Baldassarre, F., Darcet, T., Xu, H., Li, D., Szafraniec, M., Ramamonjisoa, M., and Oquab, M. Dinov2 meets text: A unified framework for image- and pixel-level vision-language alignment. *CVPR*, pp. 24905–24916, 2025.

Kang, D. and Cho, M. In defense of lazy visual grounding for open-vocabulary semantic segmentation. In *ECCV*, pp. 143–164, 2024.

Kang, S., Kim, J., Kim, J., and Hwang, S. J. Your large vision-language model only needs a few attention heads for visual grounding. In *CVPR*, pp. 9339–9350, 2025.

Karazija, L., Laina, I., Vedaldi, A., and Rupprecht, C. Diffusion models for zero-shot open-vocabulary segmentation. In *ECCV*, pp. 229–317, 2024.

Khattak, M. U., Rasheed, H., Maaz, M., Khan, S., and Khan, F. S. Maple: Multi-modal prompt learning. In *CVPR*, 2023.

Kim, C., Ju, D., Han, W., Yang, M.-H., and Hwang, S. J. Distilling spectral graph for object-context aware open-vocabulary semantic segmentation. In *CVPR*, pp. 15033–15042, 2025.

Kirillov, A., Mintun, E., Ravi, N., Mao, H., Rolland, C., Gustafson, L., Xiao, T., Whitehead, S., Berg, A. C., Lo, W.-Y., et al. Segment anything. In *ICCV*, pp. 4015–4026, 2023.

Kore, A., Abbasi Baval, E., Subasri, V., Abdalla, M., Fine, B., Dolatabadi, E., and Abdalla, M. Empirical data drift detection experiments on real-world medical imaging data. *Nature Communications*, 15(1):1887, 2024.

Krähenbühl, P. and Koltun, V. Efficient inference in fully connected CRFs with Gaussian edge potentials. In *NeurIPS*, pp. 109–117, 2011.

Lan, M., Chen, C., Ke, Y., Wang, X., Feng, L., and Zhang, W. ProxyCLIP: Proxy attention improves CLIP for open-vocabulary segmentation. In *ECCV*, pp. 70–88, 2024a.

Lan, M., Chen, C., Ke, Y., Wang, X., Feng, L., and Zhang, W. ClearCLIP: Decomposing CLIP representations for dense vision-language inference. In *ECCV*, pp. 143–160, 2024b.

Li, B., Weinberger, K. Q., Belongie, S., Koltun, V., and Ranftl, R. Language-driven semantic segmentation. In *ICLR*, 2022a.

Li, B., Dong, H., Zhang, D., Zhao, Z., Gao, J., and Li, X. Exploring efficient open-vocabulary segmentation in the remote sensing. In *AAAI*, 2026a.

Li, J., Lu, Y., Zhang, Y., Xie, Y., Wang, F., Xie, Y., and Qu, Y. Target refocusing via attention redistribution for open-vocabulary semantic segmentation: An explainability perspective. In *AAAI*, 2026b.

Li, K., Liu, R., Cao, X., Bai, X., Zhou, F., Meng, D., and Wang, Z. Segearth-ov: Towards training-free open-vocabulary segmentation for remote sensing images. In *CVPR*, pp. 10545–10556, 2025a.

Li, K., Zhang, S., Deng, Y., Wang, Z., Meng, D., and Cao, X. Segearth-ov3: Exploring sam 3 for open-vocabulary semantic segmentation in remote sensing images. *arXiv preprint arXiv:2512.08730*, 2025b.

Li, L. H., Zhang, P., Zhang, H., Yang, J., Li, C., Zhong, Y., Wang, L., Yuan, L., Zhang, L., and Hwang, J.-N. Grounded language-image pre-training. In *CVPR*, pp. 10965–10975, 2022b.

Lin, T.-Y., Maire, M., Belongie, S., Hays, J., Perona, P., Ramanan, D., Dollár, P., and Zitnick, C. L. Microsoft COCO: Common objects in context. In *ECCV*, pp. 740–755, 2014.

Liu, F., Chen, D., Guan, Z., Zhou, X., Zhu, J., Ye, Q., Fu, L., and Zhou, J. Remoteclip: A vision language foundation model for remote sensing. *TGRS*, 62:1–16, 2024.

Long, J., Shelhamer, E., and Darrell, T. Fully convolutional networks for semantic segmentation. In *CVPR*, pp. 3431–3440, 2015.

Lu, J., Liu, A., Dong, F., Gu, F., Gama, J., and Zhang, G. Learning under concept drift: A review. *TKDE*, 31(12): 2346–2363, 2018.

Luo, H., Bao, J., Wu, Y., He, X., and Li, T. SegCLIP: Patch aggregation with learnable centers for open-vocabulary semantic segmentation. In *ICML*, pp. 23033–23044, 2023.

Mottaghi, R., Chen, X., Liu, X., Cho, N.-G., Lee, S.-W., Fidler, S., Urtasun, R., and Yuille, A. The role of context for object detection and semantic segmentation in the wild. In *CVPR*, pp. 891–898, 2014.

Mukhoti, J., Lin, T.-Y., Poursaeed, O., Wang, R., Shah, A., Torr, P. H. S., and Lim, S.-N. Open vocabulary semantic segmentation with patch aligned contrastive learning. In *CVPR*, pp. 19413–19423, 2023.

Oquab, M., Dariseti, T., Moutakanni, T., Vo, H., Szafraniec, M., Khalidov, V., Fernandez, P., Haziza, D., Massa, F., and El-Nouby, A. DINOv2: Learning robust visual features without supervision. *arXiv preprint arXiv:2304.07193*, 2023.

Pratt, S., Covert, I., Liu, R., and Farhadi, A. What does a platypus look like? generating customized prompts for zero-shot image classification. In *ICCV*, 2023.

Radford, A., Kim, J. W., Hallacy, C., Ramesh, A., Goh, G., Agarwal, S., Sastry, G., Askell, A., Mishkin, P., and Clark, J. Learning transferable visual models from natural language supervision. In *ICML*, pp. 8748–8763, 2021.

Ravi, N., Gabeur, V., Hu, Y.-T., Hu, R., Ryali, C., Ma, T., Khedr, H., Rädl, R., Rolland, C., Gustafson, L., Mintun, E., Pan, J., Alwala, K. V., Carion, N., Wu, C.-Y., Girshick, R., Dollar, P., and Feichtenhofer, C. SAM 2: Segment anything in images and videos. In *ICLR*, 2025.

Rombach, R., Blattmann, A., Lorenz, D., Esser, P., and Ommer, B. High-resolution image synthesis with latent diffusion models. In *CVPR*, pp. 10684–10695, 2022.

Rousseeuw, P. J. and Hubert, M. Robust statistics for outlier detection. *Wiley Interdisciplinary Reviews: Data Mining and Knowledge Discovery*, 1(1):73–79, 2011.

Shao, T., Tian, Z., Zhao, H., and Su, J. Explore the potential of clip for training-free open vocabulary semantic segmentation. In *ECCV*, pp. 139–156, 2024.

Shi, Y., Dong, M., and Xu, C. Harnessing vision foundation models for high-performance, training-free open vocabulary segmentation. In *ICCV*, pp. 23487–23497, 2025.

Simeoni, O., Sekkat, C., Puy, G., Vobecký, A., Zablocki, E., and Pérez, P. Unsupervised object localization: Observing the background to discover objects. In *CVPR*, pp. 3176–3186, 2023.

Siméoni, O., Vo, H. V., Seitzer, M., Baldassarre, F., Oquab, M., Jose, C., Khalidov, V., Szafraniec, M., Yi, S., Ramamonjisoa, M., et al. Dinov3. *arXiv preprint arXiv:2508.10104*, 2025.

Stojnić, V., Kalantidis, Y., Matas, J., and Tolias, G. Lposs: Label propagation over patches and pixels for open-vocabulary semantic segmentation. In *CVPR*, pp. 9794–9803, 2025.

Sun, S., Li, R., Torr, P., Gu, X., and Li, S. CLIP as RNN: Segment countless visual concepts without training endeavor. In *CVPR*, pp. 13171–13182, 2024.

Tu, W., Deng, W., and Gedeon, T. A closer look at the robustness of contrastive language-image pre-training (CLIP). In *NeurIPS*, pp. 13678–13691, 2023.

Wang, F., Mei, J., and Yuille, A. SCLIP: Rethinking self-attention for dense vision-language inference. In *ECCV*, pp. 315–332, 2024a.

Wang, H., Vasu, P. K. A., Faghri, F., Vemulapalli, R., Farajtabar, M., Mehta, S., Rastegari, M., Tuzel, O., and Pouransari, H. Sam-clip: Merging vision foundation models towards semantic and spatial understanding. In *CVPRW*, pp. 3635–3647, 2024b.

Wang, J., Zheng, Z., Ma, A., Lu, X., and Zhong, Y. Loveda: A remote sensing land-cover dataset for domain adaptive semantic segmentation. *arXiv preprint arXiv:2110.08733*, 2021.

Wang, X., Girdhar, R., Yu, S. X., and Misra, I. Cut and learn for unsupervised object detection and instance segmentation. In *Proceedings of the IEEE Conference on Computer Vision and Pattern Recognition (CVPR)*, pp. 3124–3134, 2023.

Wang, Y., Shen, X., Hu, S. X., Yuan, Y., Crowley, J. L., and Vaufreydaz, D. Self-supervised transformers for unsupervised object discovery using normalized cut. In *CVPR*, pp. 14343–14353, 2022.

Waqas Zamir, S., Arora, A., Gupta, A., Khan, S., Sun, G., Shahbaz Khan, F., Zhu, F., Shao, L., Xia, G.-S., and Bai, X. issaid: A large-scale dataset for instance segmentation in aerial images. In *CVPRW*, pp. 28–37, 2019.

Wu, J.-J., Chang, A. C.-H., Chuang, C.-Y., Chen, C.-P., Liu, Y.-L., Chen, M.-H., Hu, H.-N., Chuang, Y.-Y., and Lin, Y.-Y. Image-text co-decomposition for text-supervised semantic segmentation. In *CVPR*, pp. 26794–26803, 2024.

Wysoczanska, M., Simeoni, O., Ramamonjisoa, M., Bursuc, A., Trzcinski, T., and Perez, P. CLIP-DINOiser: Teaching CLIP a few DINO tricks for open-vocabulary semantic segmentation. In *ECCV*, pp. 320–337, 2024.

Xie, B., Cao, J., Xie, J., Khan, F. S., and Pang, Y. SED: A simple encoder-decoder for open-vocabulary semantic segmentation. In *CVPR*, pp. 3426–3436, 2024.

Xie, E., Wang, W., Yu, Z., Anandkumar, A., Alvarez, J. M., and Luo, P. Segformer: Simple and efficient design for semantic segmentation with transformers. In *NeurIPS*, pp. 12077–12090, 2021.

Xu, J., Mello, S. D., Liu, S., Byeon, W., Breuel, T., Kautz, J., and Wang, X. GroupViT: Semantic segmentation emerges from text supervision. In *CVPR*, pp. 18134–18144, 2022a.

Xu, M., Zhang, Z., Wei, F., Lin, Y., Cao, Y., Hu, H., and Bai, X. A simple baseline for open-vocabulary semantic segmentation with pre-trained vision-language model. In *ECCV*, pp. 736–753, 2022b.

Xu, M., Zhang, Z., Wei, F., Hu, H., and Bai, X. Side adapter network for open-vocabulary semantic segmentation. In *CVPR*, pp. 2945–2954, 2023.

Xuan, X., Deng, Z., and Ma, K.-L. Reme: A data-centric framework for training-free open-vocabulary segmentation. In *ICCV*, pp. 20954–20965, 2025.

Zhang, D., Liu, F., and Tang, Q. Corrclip: Reconstructing patch correlations in clip for open-vocabulary semantic segmentation. In *ICCV*, pp. 24677–24687, 2025.

Zhang, R., Wei, Z., Fang, R., Gao, P., Li, K., Dai, J., Qiao, Y., and Li, H. Tip-adapter: Training-free adaption of clip for few-shot classification. In *ECCV*, 2022.

Zhao, H., Puig, X., Zhou, B., Fidler, S., and Torralba, A. Open vocabulary scene parsing. In *ICCV*, pp. 2002–2010, 2017.

Zhong, Y., Yang, J., Zhang, P., Li, C., Codella, N., Li, L. H., Zhou, L., Dai, X., Yuan, L., and Li, Y. RegionCLIP: Region-based language-image pretraining. In *CVPR*, pp. 16793–16803, 2022.

Zhou, B., Zhao, H., Puig, X., Fidler, S., Barriuso, A., and Torralba, A. Scene parsing through ADE20K dataset. In *CVPR*, pp. 633–641, 2017.

Zhou, C., Loy, C. C., and Dai, B. Extract free dense labels from CLIP. In *ECCV*, pp. 350–368, 2022a.

Zhou, K., Yang, J., Loy, C. C., and Liu, Z. Conditional prompt learning for vision-language models. In *CVPR*, 2022b.

Zhou, X., Girdhar, R., Joulin, A., Krähenbühl, P., and Misra, I. Detecting twenty-thousand classes using image-level supervision. In *ECCV*, pp. 350–368, 2022c.

Zhu, Q., Lao, J., Ji, D., Luo, J., Wu, K., Zhang, Y., Ru, L., Wang, J., Chen, J., Yang, M., et al. Skysense-o: Towards open-world remote sensing interpretation with vision-centric visual-language modeling. In *CVPR*, pp. 14733–14744, 2025.

Zou, X., Dou, Z.-Y., Yang, J., Gan, Z., Li, L., Li, C., Dai, X., Behl, H., Wang, J., and Yuan, L. Generalized decoding for pixel, image, and language. In *CVPR*, pp. 15116–15127, 2023a.

Zou, X. et al. Segment everything everywhere all at once. *arXiv preprint arXiv:2304.06718*, 2023b.

## Appendix

### A. Additional Ablations

This section reports additional ablations omitted from the main paper due to space constraints. All settings follow §3.1 with SAM3 fully frozen and identical data splits. Unless otherwise stated, we use the same benchmark grouping as the main paper: **NS** (Natural-Scene) and **RS** (Remote-Sensing), and report **Avg. mIoU**.

#### A.1. Sensitivity to Representative Mining: $\text{Top}_K$

Stage II (§2.2) trims atypical supports by retaining the  $K$  crops that are most consistent with the target prototype (Eq. (6)). In our implementation,  $\text{Top}_K$  corresponds to the per-class budget of representative crops collected in Stage II. We ablate  $K$  over a broad range. When a class contains fewer than  $K$  supports, we use all available crops.

Table 6.  $\text{Top}_K$  sensitivity in Stage II. **NS** and **RS** denote Natural-Scene and Remote-Sensing benchmarks.

$K$	1	5	10	30	50	100
<b>NS Avg. mIoU</b>	61.7	63.3	<b>64.7</b>	64.1	64.5	64.3
<b>RS Avg. mIoU</b>	48.1	51.0	52.1	52.3	<b>52.5</b>	51.8

$\text{Top}_K$  controls a robustness-coverage trade-off: smaller  $K$  yields a tighter “core” (stronger trimming), while larger  $K$  increases appearance coverage but risks re-introducing outliers and background-dominated crops. In practice, performance is typically stable within a mid-range of  $K$ , motivating a single default ( $K = 10$ ) used in the main paper.

#### A.2. Sensitivity to Concept Fusion: $\text{Top}_J$

Stage III aggregates candidate prompt embeddings via temperature-scaled soft fusion (Eq. (8)). In our implementation, we set  $J$  to include *all* expanded prompt candidates for each class, and rely on score-based weighting (and a light gating rule) to downweight borderline prompts rather than hard-truncating the pool. We also report a  $\text{Top}_J$  sweep by explicitly restricting the fusion to the  $\text{Top}_J$  candidates ranked by the concept scoring in Eq. (7). When  $J=1$ , Eq. (8) degenerates to selecting a single best prompt embedding.

Table 7.  $\text{Top}_J$  sensitivity in Stage III.  $J=1$  denotes single-prompt selection without fusion, while **All** uses the full expanded prompt set.

$J$	1	2	4	8	16	All
<b>NS Avg. mIoU</b>	60.6	61.5	63.6	64.5	64.5	<b>64.7</b>
<b>RS Avg. mIoU</b>	48.1	49.7	50.1	51.7	<b>52.1</b>	<b>52.1</b>

Restricting fusion to a small  $J$  reduces prompt-level variance and can prevent weak candidates from entering the mixture. In contrast, using **All** maximizes linguistic coverage and lets the temperature-scaled weights suppress low-scoring prompts automatically, which is the default setting in our main experiments.

#### A.3. Concept Scoring Metric: Dice vs. IoU

In Eq. (7), the main paper uses **Dice** to score candidate prompts on representative supports. We ablate the scoring metric by replacing **Dice** with **IoU** while keeping all other steps unchanged. We report this comparison in Table 8. **Dice** is often numerically more stable on small or thin structures due to its symmetric overlap form, whereas **IoU** is stricter and can be more sensitive to boundary errors.

Table 8. Concept scoring in Stage III: **Dice** vs. **IoU** (cf. Eq. (7)).

Scoring metric	NS Avg. mIoU	RS Avg. mIoU
<b>Dice (main)</b>	<b>64.7</b>	<b>52.1</b>
IoU	62.9	51.0

## B. Concept Bank Construction Cost

We report the one-time offline cost to construct CONCEPTBANK on the target support split. This cost is *not* included in the inference efficiency comparison (Table 5), since CONCEPTBANK is built once per dataset and then reused for all inference runs. We measure wall-clock time of Stages I-III (§2.2) on the support split: (i) mask-pooled crop embeddings and prototype estimation (Stage I), (ii) representative support mining (Stage II), (iii) candidate scoring and fusion (Stage III).

Table 9. One-time CONCEPTBANK construction time per dataset (target support split, *i.e.*, training set).

Dataset	$ \mathcal{C} $	#Imgs	$M$	Crops	Stage I (min)	Stage II (min)	Stage III (min)	Total (min)
V21 (Everingham et al., 2015)	21	1,464	27	840	0.99	1.00	1.03	3.02
PC60 (Mottaghi et al., 2014)	60	4,996	6	2,399	2.68	2.83	1.63	7.14
COCO-O (Lin et al., 2014)	80	118,287	40	3,240	4.32	4.61	2.62	11.55
V20 (Everingham et al., 2015)	20	1,464	14	800	0.88	0.94	0.72	2.55
PC59 (Mottaghi et al., 2014)	59	4,996	6	2,359	2.63	2.78	1.65	7.07
COCO-S (Caesar et al., 2018)	171	118,287	6	6,840	8.43	8.89	4.80	22.12
City (Cordts et al., 2016)	19	2,975	9	760	1.25	1.50	0.79	3.53
ADE (Zhou et al., 2017)	150	20,210	6	5,996	6.84	7.49	4.23	18.56
LoveDA (Wang et al., 2021)	7	2,522	12	2,800	1.70	0.22	0.35	2.27
Potsdam (ISPRS, 2012a)	6	3,456	4	2,400	1.33	0.73	0.66	2.72
Vaihingen (ISPRS, 2012b)	6	344	4	1,025	0.57	0.66	0.64	1.87
iSAID (Waqas Zamir et al., 2019)	16	33,978	6	6,282	5.51	0.64	0.42	6.56

Stage I is dominated by visual feature extraction over masked crops and scales with the total number of crop pixels. Stage III scales with  $\sum_c |\mathcal{R}_c| \cdot M$  forward evaluations of  $f_\Phi$  on representative supports. Both stages are embarrassingly parallel across classes and supports, and benefit from batching and mixed precision.

## C. Pseudo-code for Concept Bank Construction

```

# =====
# ConceptBank Construction
# =====
# Inputs:
#   D_train : target support set with images and GT masks
#   C       : class set
#   Phi     : frozen SAM3; provides f_Phi (mask predictor), phi_T (text encoder),
#             and the dense visual features used in mask pooling
#   Docs   : dataset documentation / label definitions (text)
# Hyper-params:
#   K : Top-K for representative mining
#   M : #candidate prompts per class (prompt expansion size)
#   J : Top-J for fusion
#   tau : softmax temperature for fusion

def build_concept_bank(D_train, C, Phi, Docs, K, M, J, tau):
    B = {} # concept bank: class -> calibrated embedding e*_c
    # --- Stage I: Prototype Estimation ---
    # Collect mask-pooled crop embeddings per class
    Z = {c: [] for c in C} # list of z(v,y) for each class
    for (x, Y) in D_train:
        for c in C:
            if has_instance(Y[c]):
                for (v, y_crop) in extract_instance_crops(x, Y[c]):
                    z = mask_pooled_embedding(Phi, v, y_crop) # Eq.(6)
                    Z[c].append(z)
    P = {}
    for c in C:
        P[c] = l2_normalize(mean(Z[c])) # prototype p_c, Eq.(7)

    # --- Stage II: Representative Support Mining (Top-K) ---
    R = {}
    for c in C:
        scores = [cos(z, P[c]) for z in Z[c]]
        idx = topk_indices(scores, k=min(K, len(scores)))
        R[c] = idx # store indices of representative supports in Z[c]

    # --- Stage III: Prototype-consistent Concept Fusion ---
    for c in C:
        # Concept Pooling (prompt expansion from docs; text-only rewriting)
        Tc = prompt_expand(class_name=c, docs=Docs, M=M) # list of strings
        Ec = [Phi.phi_T(t) for t in Tc] # prompt embeddings

        # Concept Scoring (functional scoring via segmentation on R_c)
        S = []
        for m, e_cm in enumerate(Ec):
            dices = []
            for idx in R[c]:
                v, y = fetch_crop_and_mask(D_train, c, idx)
                y_hat = Phi.f_Phi(v, e_cm)
                dices.append(dice(y_hat, y)) # Eq.(10); or IoU in ablation
            S.append(mean(dices))

        # Top-J + soft fusion
        Jc = topj_indices(S, j=min(J, len(S)))
        w = softmax([S[j]/tau for j in Jc])
        e_star = sum(wi * l2_normalize(Ec[j]) for wi, j in zip(w, Jc))
        B[c] = e_star

    return B

```

## D. Prompt Expansion Protocol and Generation Prompts

We expand each class name into a set of synonym- and attribute-enriched prompts using an off-the-shelf LLM. The LLM is provided with dataset documentation (original paper, label taxonomy, and official label definitions). The generation is constrained to *text-level rewriting* of the given label semantics and does not introduce new visual concepts beyond the dataset definition.

### D.1. Quality-control rules

We apply the following constraints to ensure label-faithful prompt expansion: (i) preserve the original class semantics; avoid adding new objects/scenes; (ii) allow synonyms, spelling variants (US/UK), plural/singular, and short attribute phrases that are consistent with the label definition; (iii) remove overly broad hypernyms if they may cause class leakage (e.g., replacing a fine-grained class with “animal”); (iv) deduplicate near-identical strings; (v) keep a fixed budget  $M$  per class.

### D.2. LLM prompt templates

#### Template (Natural-scene datasets).

**System:** You are an expert dataset annotator for open-vocabulary segmentation. You must follow label definitions strictly and avoid introducing new visual concepts.

**User:** You are given (1) a dataset name, (2) a class name, and (3) official label documentation. Generate a comma-separated list of prompt variants that stay within the same class semantics.

*Input:* Dataset: {DATASET} Class name: {CLASS} Label documentation (authoritative): {DOCS}

*Rules:* - Output format: a single line, comma-separated phrases, no numbering, no extra text. - Include: synonyms, spelling variants, common subtypes, and short attribute phrases consistent with the documentation. - Do NOT add any object that is not implied by the documentation. - Avoid overly generic words that could overlap many classes (e.g., “thing”, “object”). - Keep 2-16 items total (including the original class name). - Prefer concise noun phrases (1-4 words).

#### Template (Remote-sensing datasets).

**System:** You are an expert dataset annotator for aerial/remote-sensing semantic segmentation. Follow dataset label definitions. Keep prompts consistent with top-down imagery and surface appearance.

**User:** Given the dataset label documentation, expand the class name into a comma-separated list of synonyms and attribute-enriched phrases that are label-faithful for aerial imagery.

*Input:* Dataset: {DATASET} Class name: {CLASS} Label documentation (authoritative): {DOCS}

*Rules:* - Output a single comma-separated line; no extra commentary. - Allow: synonyms, material/surface descriptors (e.g., asphalt road), and aerial terms (e.g., roof, canopy) *only if* they are consistent with the class definition. - Do NOT introduce new land-cover categories not present in the documentation. - Keep 1-15 items total (including the original class name).

### D.3. Prompt Expansion Statistics

Table 10 reports summary statistics of the expanded concept candidates per class. Natural-scene object categories typically admit more lexical variants, while several remote-sensing benchmarks remain comparatively compact.

Table 10. Prompt expansion statistics. Counts are per-class candidate concepts (incl. the original class name).

Stat.	Natural-Scene								Remote-Sensing			
	V21	V20	PC60	PC59	COCO-O	COCO-S	City	ADE	LoveDA	Potsdam	Vaihingen	iSAID
$ \mathcal{C} $	21	20	60	59	81	171	19	150	7	6	6	16
Min	4	4	3	3	2	2	4	3	4	2	2	1
Max	27	14	6	6	40	6	9	6	12	4	4	6
Avg.	9.29	8.40	4.67	4.64	5.47	4.93	6.32	4.83	8.00	2.67	3.17	3.50

## E. Additional Quantitative Results

We further compare against a recent SAM3-based approach, SegEarth-OV3 (Li et al., 2025b), on both natural-scene (NS) benchmarks (Table. 11) and remote-sensing (RS) benchmarks (Table. 12). Across the two groups, CONCEPTBANK improves the average mIoU by **+4.1** on NS and **+3.7** on RS. We note that SegEarth-OV3 relies on manually rewritten category names; in our re-checks, even small edits to a subset of class names can noticeably degrade its performance, suggesting a higher sensitivity to prompt phrasing. It is also substantially slower at inference time, since it follows the standard SAM3 text-encoding pipeline and requires running the text encoder and grounding repeatedly per class (and even more when multiple prompts are used). In contrast, our Concept Bank is constructed offline and stores the calibrated text representations, so inference *bypasses the text encoder entirely* (see §3.3) and scores all labels for each sample in a single forward pass, yielding a clear speed advantage (often by several to tens of times) while improving robustness under drift.

*Table 11. Quantitative comparison of OVS on natural-scene datasets.* “Parameter-free” denotes methods without learnable parameters or gradient-based optimization. Metric values are mIoU (%). **bold** and underlined indicate the best and second-best results, respectively.

Method	Pub. & Year	Backbone (Size)	with background			without background			Avg.
			V21	PC60	COCO-O	V20	PC59	COCO-S	
<b>Training-based</b>									
GroupViT (Xu et al., 2022a)	CVPR’22	GroupViT (ViT-S/16)	50.4	18.7	27.5	79.7	23.4	15.3	11.1
TCL (Cha et al., 2023)	CVPR’23	CLIP	51.2	24.3	30.4	77.5	30.3	19.6	23.1
SegCLIP (Luo et al., 2023)	ICML’23	CLIP	52.6	24.7	27.5	-	-	-	-
CoDe (Wu et al., 2024)	CVPR’24	CLIP	57.7	30.5	32.3	-	-	23.9	28.9
SAM-CLIP (Wang et al., 2024b)	CVPR’24	CLIP + SAM (ViT-B/16)	60.6	29.2	-	-	-	31.5	17.1
Talk2DINO (Barsellotti et al., 2025)	ICCV’25	CLIP + DINOv2 <sup>†</sup> (ViT-B/14)	65.8	37.7	45.1	88.5	42.4	30.2	38.1
<b>Parameter-free</b>									
NACLIP* (Hajimiri et al., 2025)	WACV’25	CLIP	58.9	32.2	33.2	79.7	35.2	23.3	35.5
LPOSS (Stojnić et al., 2025)	CVPR’25	CLIP + DINO (ViT-B/16)	61.1	34.6	33.4	78.8	37.8	25.9	37.3
CASS* (Kim et al., 2025)	CVPR’25	CLIP + DINO (ViT-B/8)	65.8	36.7	37.8	87.8	40.2	26.7	39.4
$\mathcal{DTH}$ -CLIP (Duan et al., 2025)	ICCV’25	CLIP	64.2	36.0	37.4	84.9	39.7	26.7	40.2
SFP (Jin et al., 2025) (Jin et al., 2025)	ICCV’25	CLIP	63.9	37.2	37.9	84.5	39.9	26.4	41.1
CorrCLIP (Zhang et al., 2025)	ICCV’25	CLIP (ViT-L/14) + DINO (ViT-B/8) + SAM2 (Hiera-L)	76.7	44.9	49.4	91.5	50.8	34.0	51.1
Trident (Shi et al., 2025)	ICCV’25	CLIP + DINO (ViT-B/16) + SAM (ViT-B/16)	67.1	38.6	41.1	84.5	42.2	28.3	42.9
ReME (Xuan et al., 2025)	ICCV’25	CLIP + DINOv2 (ViT-L/14) + SAM (ViT-L/16)	82.2	44.6	48.2	93.2	53.1	33.3	59.0
RF-CLIP (Li et al., 2026b)	AAAI’26	CLIP	67.2	37.9	39.1	87.0	41.4	27.5	43.0
SAM3* (Carion et al., 2026)	ICLR’26	SAM3 (PE-L+/14)	<u>81.9</u>	46.1	65.4	88.9	50.0	33.3	62.3
SegEarth-OV3* (Li et al., 2025b)	arXiv’25	SAM3 (PE-L+/14)	79.8	50.7	<u>67.6</u>	<u>96.8</u>	<u>58.8</u>	42.8	<u>69.7</u>
<b>CONCEPTBANK (Ours)</b>	-	SAM3 (PE-L+/14)	<b>87.1</b>	<b>56.5</b>	<b>67.9</b>	<b>97.4</b>	<b>63.0</b>	<b>46.4</b>	<b>75.1</b>

*Notes:* Unless otherwise specified, CLIP uses ViT-B/16 (Dosovitskiy et al., 2021). “\*” denotes results reproduced in our work. “<sup>†</sup>” indicates DINOv2 equipped with registers (Dariset al., 2024). “-” indicates results are not reported or applicable in the original paper.

*Table 12. Quantitative comparison of OVS on remote-sensing datasets.* “Parameter-free” denotes methods without learnable parameters or gradient-based optimization. Metric values are mIoU (%). **bold** and underlined indicate the best and second-best results, respectively.

Method	Pub. & Year	Backbone (Size)	with background				Avg.
			LoveDA	Potsdam	Vaihingen	iSAID	
<b>Training-based</b>							
SAN (Xu et al., 2023)	CVPR’23	CLIP (ViT-L/14@336px)	25.3	37.3	39.2	<u>49.6</u>	37.9
Cat-Seg (Cho et al., 2024)	CVPR’24	CLIP (ViT-L/14@336px)	28.6	35.8	42.3	<u>53.3</u>	40.0
SkySense-O (Zhu et al., 2025)	CVPR’25	CLIP (ViT-L/14@512px)	38.3	54.1	51.6	43.9	47.0
RSKT-Seg (Li et al., 2026a)	AAAI’26	CLIP (ViT-L/14@336px) + RemoteCLIP <sup>†</sup> (ViT-B/16) + DINO (ViT-B/32)	33.2	38.4	42.7	<b>54.3</b>	42.2
<b>Parameter-free</b>							
CLIP (Radford et al., 2021)	ICML’21	CLIP	12.4	15.6	10.8	7.5	11.6
MaskCLIP (Zhou et al., 2022a)	ECCV’22	CLIP	27.8	33.9	29.9	14.5	26.5
GEM (Bousselham et al., 2024)	CVPR’24	CLIP	31.6	39.1	36.4	17.7	31.2
ProxyCLIP (Lan et al., 2024a)	ECCV’24	CLIP + DINOv2 <sup>†</sup> (ViT-B/14)	34.3	49.0	47.5	21.8	38.2
SCLIP* (Wang et al., 2024a)	ECCV’24	CLIP	30.4	39.6	35.9	16.1	30.5
SegEarth-OV* (Li et al., 2025a)	CVPR’25	CLIP	36.9	48.5	40.0	21.7	36.8
CorrCLIP* (Zhang et al., 2025)	ICCV’25	CLIP + DINO (ViT-B/8) + SAM2 (Hiera-L)	36.9	51.9	47.0	25.5	40.3
SAM3* (Carion et al., 2026)	ICLR’26	SAM3 (PE-L+/14)	35.6	54.1	49.1	17.7	39.1
SegEarth-OV3* (Li et al., 2025b)	arXiv’25	SAM3 (PE-L+/14)	<u>47.4</u>	<u>57.8</u>	<u>60.8</u>	27.6	<u>48.4</u>
<b>CONCEPTBANK (Ours)</b>	-	SAM3 (PE-L+/14)	<b>49.4</b>	<b>60.5</b>	<b>63.0</b>	35.4	<b>52.1</b>

*Notes:* Unless otherwise specified, CLIP uses ViT-B/16 (Dosovitskiy et al., 2021). “\*” denotes results reproduced in our work. “<sup>†</sup>” indicates DINOv2 equipped with registers. “<sup>†</sup>” indicates RemoteCLIP (Liu et al., 2024), a CLIP-based remote sensing foundation model.

## F. Additional Qualitative Results

We present additional qualitative comparisons between the original SAM3 baseline and our CONCEPTBANK on both Natural-Scene (see Figs. 5-12) and Remote-Sensing (see Figs. 13-16) benchmarks. As shown in Figs. 5-16, CONCEPTBANK effectively reduces spurious activations caused by distribution shifts. We also observe cases in which both methods produce visually plausible segmentations that are more consistent with object boundaries than the provided annotations.



Figure 5. Qualitative comparison results of open-vocabulary segmentation on Pascal VOC21. Zoom in for best view.

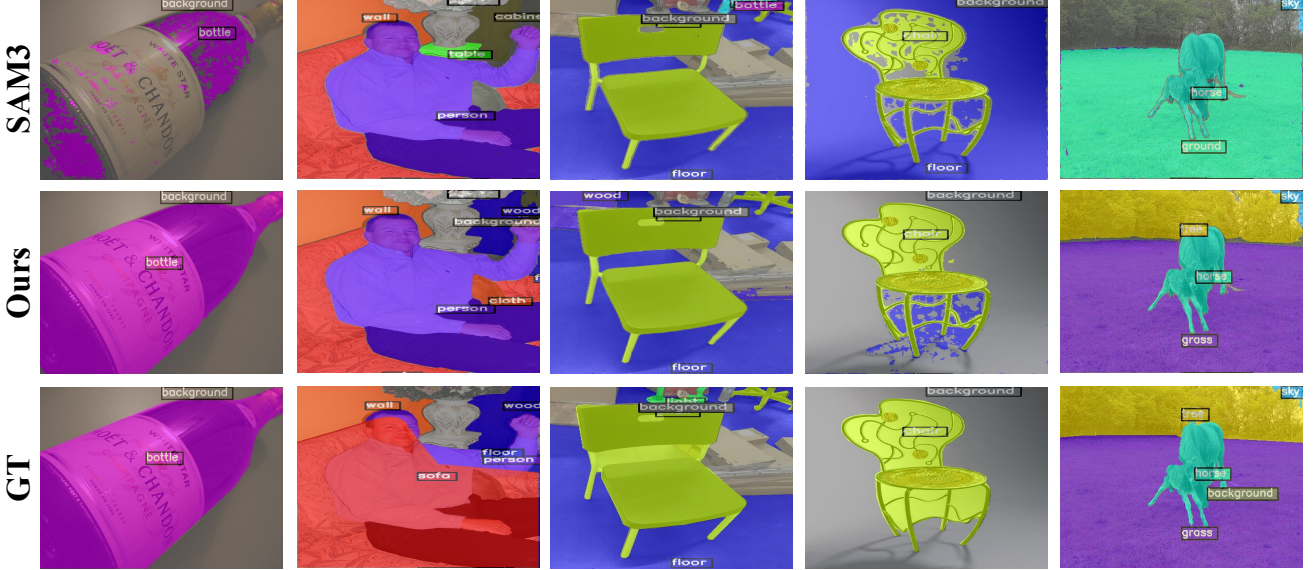


Figure 6. Qualitative comparison results of open-vocabulary segmentation on Pascal Context 60. Zoom in for best view.



Figure 7. Qualitative comparison results of open-vocabulary segmentation on COCO-Object. Zoom in for best view.



Figure 8. Qualitative comparison results of open-vocabulary segmentation on Pascal VOC 20. Zoom in for best view.

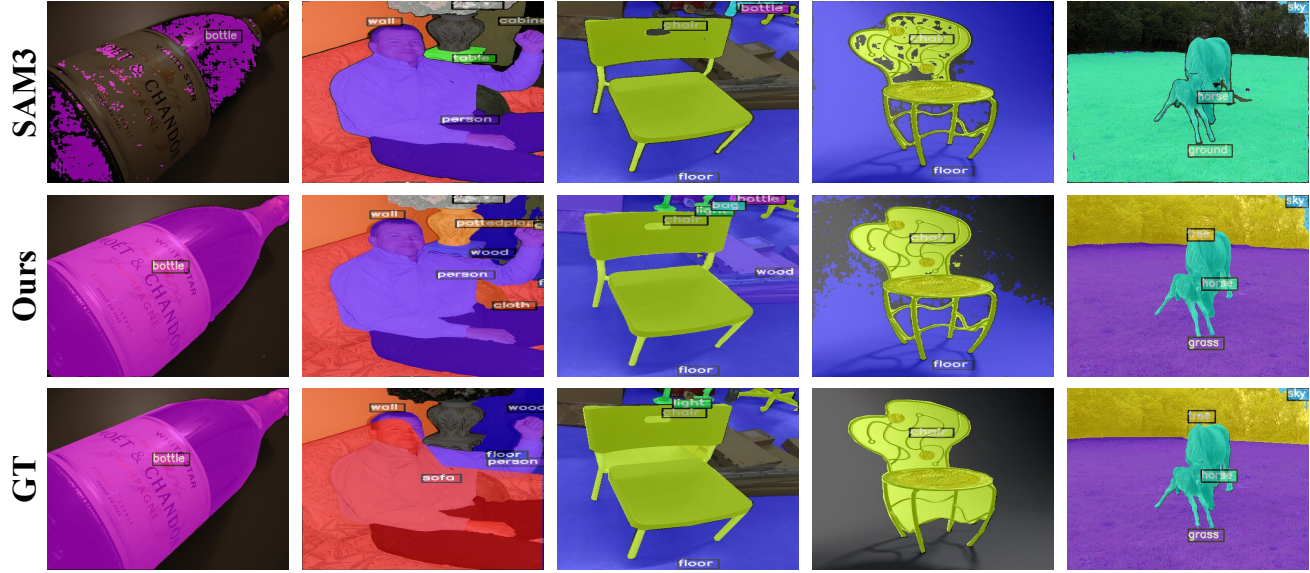


Figure 9. Qualitative comparison results of open-vocabulary segmentation on Pascal Context 59. Zoom in for best view.



Figure 10. Qualitative comparison results of open-vocabulary segmentation on COCO-Stuff. Zoom in for best view.



Figure 11. Qualitative comparison results of open-vocabulary segmentation on Cityscapes. Zoom in for best view.

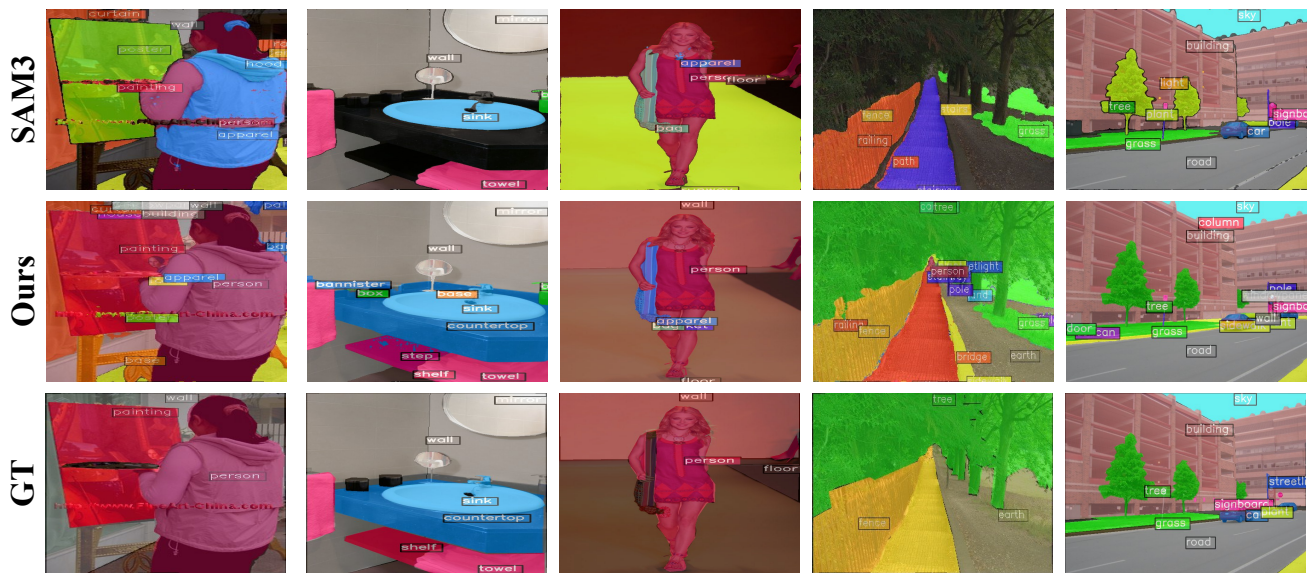


Figure 12. Qualitative comparison results of open-vocabulary segmentation on ADE20K. Zoom in for best view.

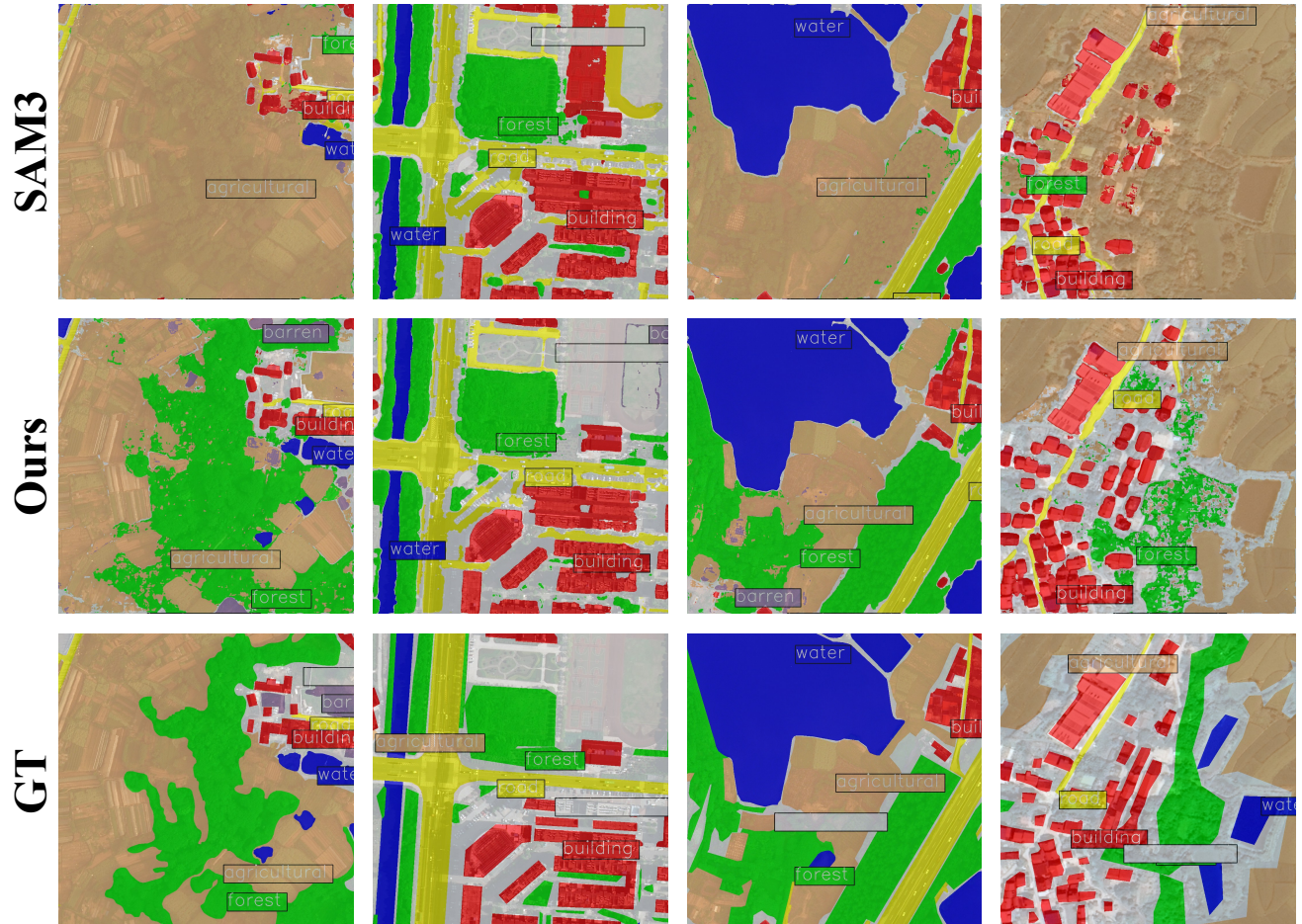


Figure 13. Qualitative comparison results of open-vocabulary segmentation on LoveDA. Zoom in for best view.

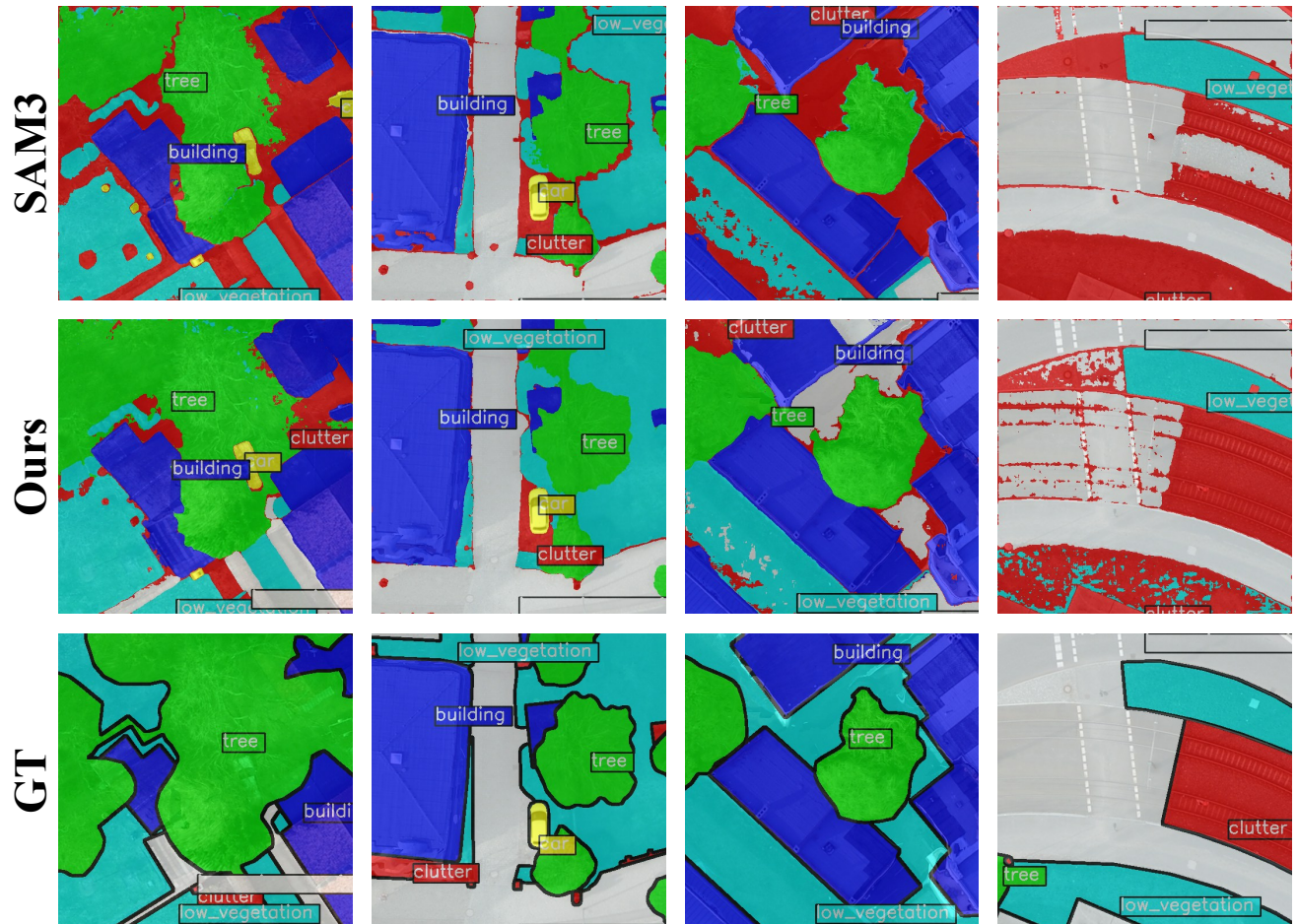


Figure 14. Qualitative comparison results of open-vocabulary segmentation on Potsdam. Zoom in for best view.

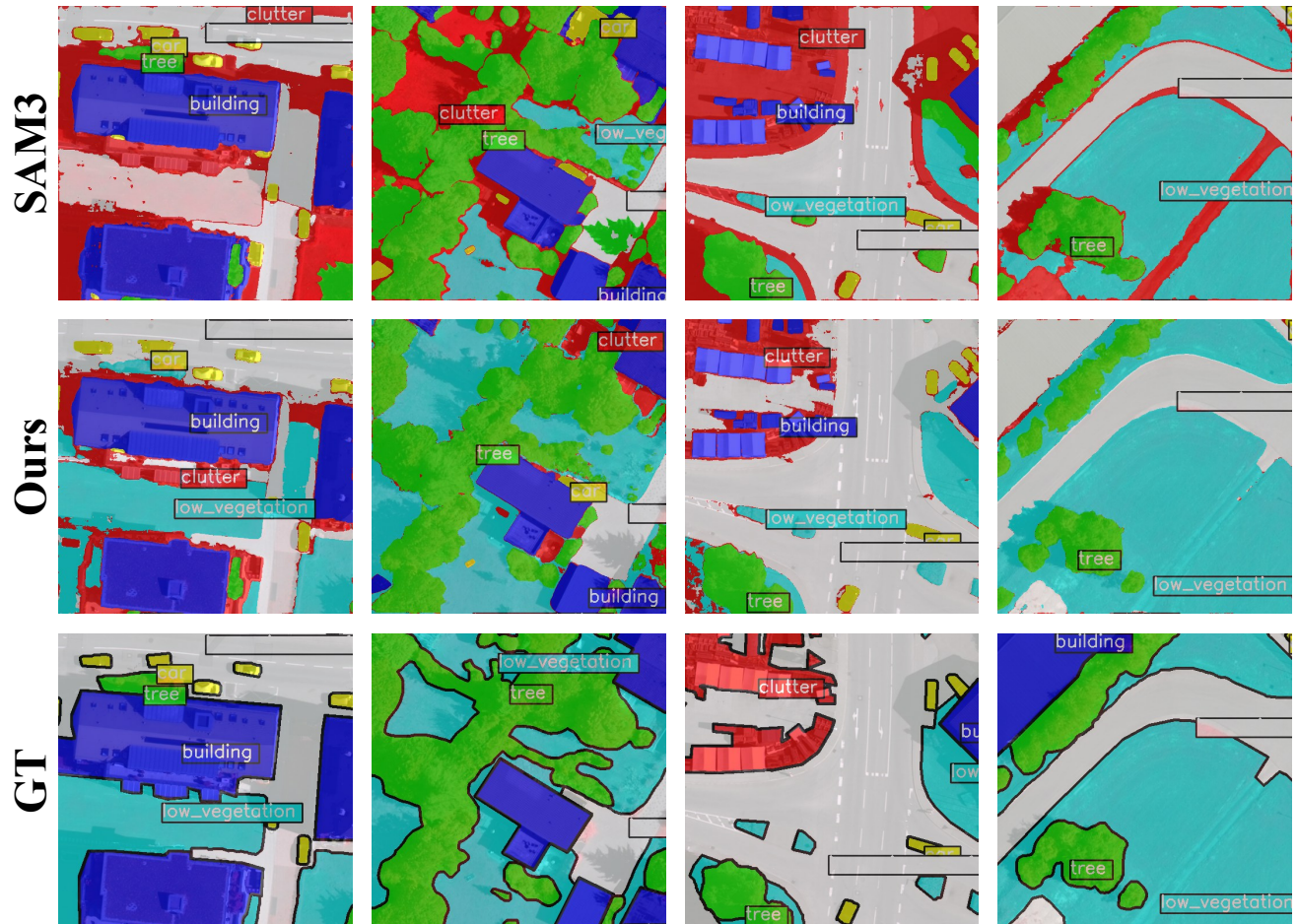


Figure 15. Qualitative comparison results of open-vocabulary segmentation on Vaihingen. Zoom in for best view.

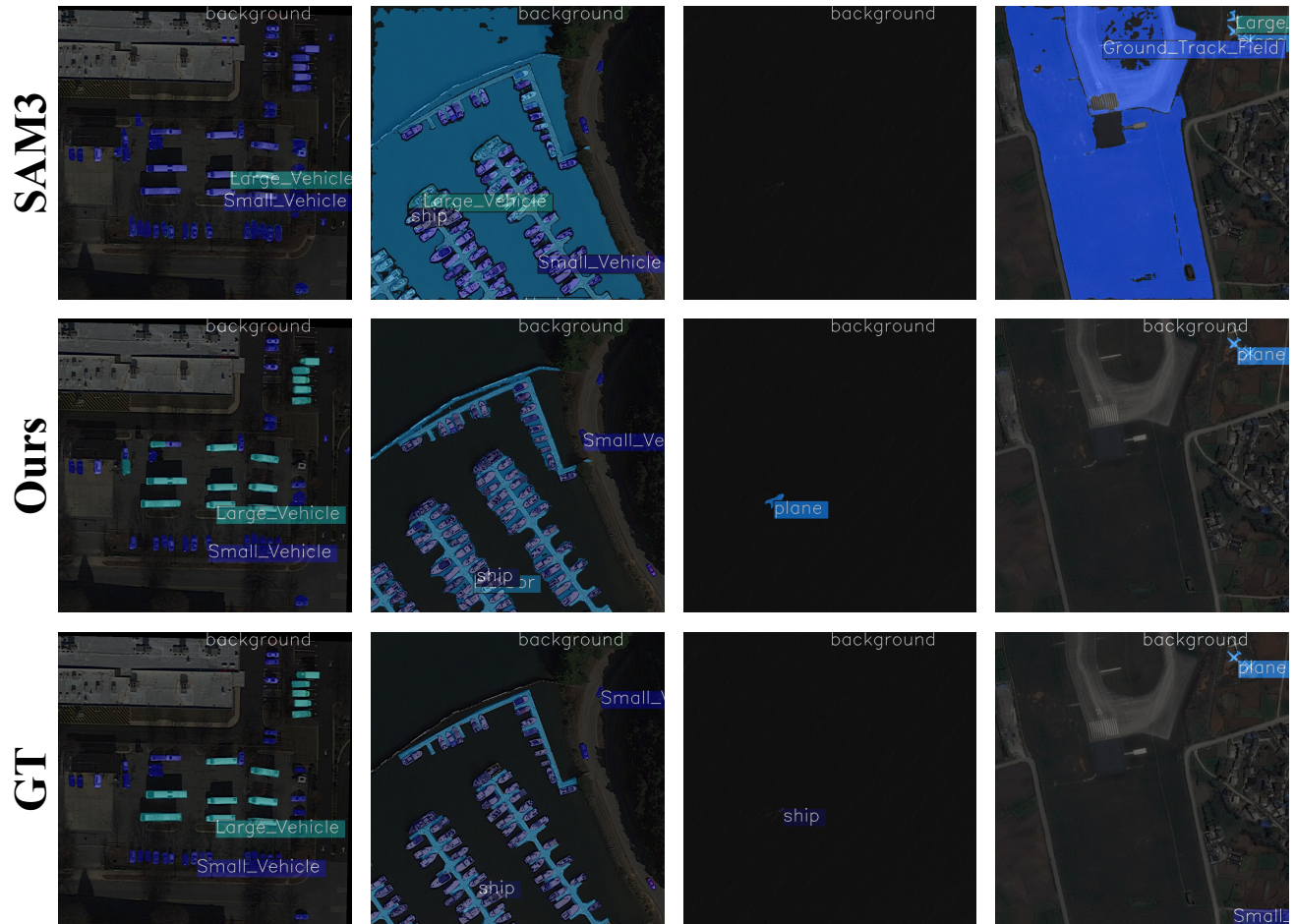


Figure 16. Qualitative comparison results of open-vocabulary segmentation on iSAID. Zoom in for best view.